Article

Cell Reports

Hierarchical RNA Processing Is Required for Mitochondrial Ribosome Assembly

Graphical Abstract

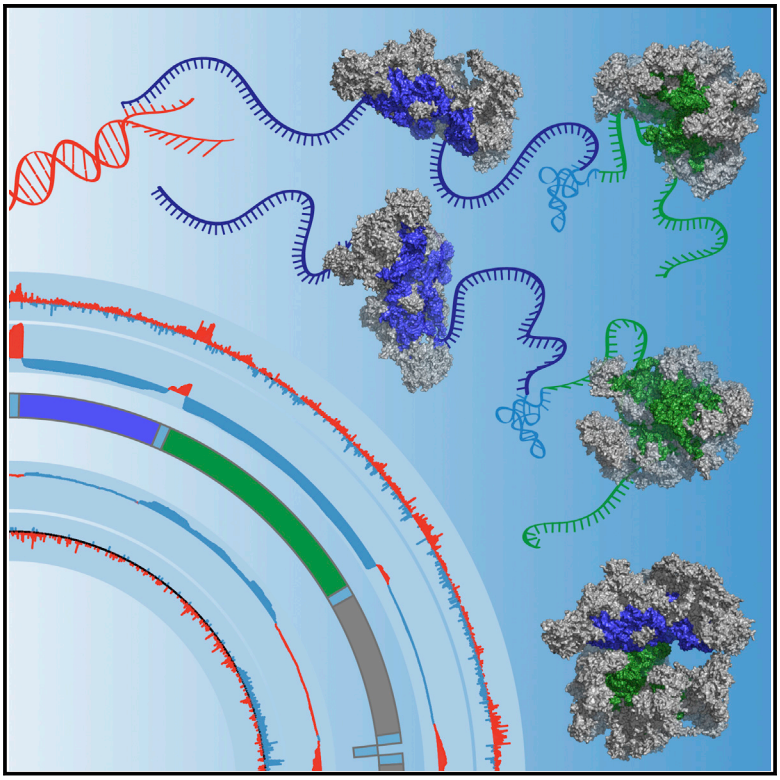

Authors

Oliver Rackham, Jakob D. Busch, Stanka Matic, ..., Dusanka Milenkovic, Nils-Göran Larsson, Aleksandra Filipovska

Correspondence

aleksandra.filipovska@uwa.edu.au

In Brief

Rackham et al. generate conditional knockout mice lacking the endoribonuclease component of the mitochondrial RNase P and show it is essential. They show that 5′ tRNA cleavage precedes 3′ processing and that processing is required for mitoribosome biogenesis. They find that RNA processing links transcription to translation via mitoribosome assembly.

Highlights

- MRPP3 is essential and its activity is non-redundant in mitochondria
- 5′ tRNA cleavage precedes 3′ end processing in vivo
- RNA processing is required for biogenesis of mitoribosomes
- RNA processing links transcription to translation via mitoribosome assembly

Accession Numbers

GSE83471

Rackham et al., 2016, Cell Reports *16*, 1874–1890
August 16, 2016
http://dx.doi.org/10.1016/j.celrep.2016.07.031

CellPress

OPEN ACCESS
CellPress

Cell Reports
Article

Hierarchical RNA Processing Is Required for Mitochondrial Ribosome Assembly

Oliver Rackham,[1,2] Jakob D. Busch,[3] Stanka Matic,[3] Stefan J. Siira,[1] Irina Kuznetsova,[1] Ilian Atanassov,[4] Judith A. Ermer,[1] Anne-Marie J. Shearwood,[1] Tara R. Richman,[1] James B. Stewart,[3] Arnaud Mourier,[3,5] Dusanka Milenkovic,[3] Nils-Göran Larsson,[3,6] and Aleksandra Filipovska[1,2,*]

[1]Harry Perkins Institute of Medical Research and Centre for Medical Research
[2]School of Chemistry and Biochemistry
The University of Western Australia, Nedlands, WA 6009, Australia
[3]Department of Mitochondrial Biology, Max Planck Institute for Biology of Ageing, 50931 Cologne, Germany
[4]Proteomics Core Facility, Max Planck Institute for Biology of Ageing, D-50931 Cologne, Germany
[5]CNRS, Institut de Biochimie et Génétique Cellulaires UMR 5095, Saint-Saëns, 33077 Bordeaux, France
[6]Department of Medical Biochemistry and Biophysics, Karolinska Institutet, Stockholm 17177, Sweden
*Correspondence: aleksandra.filipovska@uwa.edu.au
http://dx.doi.org/10.1016/j.celrep.2016.07.031

SUMMARY

The regulation of mitochondrial RNA processing and its importance for ribosome biogenesis and energy metabolism are not clear. We generated conditional knockout mice of the endoribonuclease component of the RNase P complex, MRPP3, and report that it is essential for life and that heart and skeletal-muscle-specific knockout leads to severe cardiomyopathy, indicating that its activity is non-redundant. Transcriptome-wide parallel analyses of RNA ends (PARE) and RNA-seq enabled us to identify that in vivo 5′ tRNA cleavage precedes 3′ tRNA processing, and this is required for the correct biogenesis of the mitochondrial ribosomal subunits. We identify that mitoribosomal biogenesis proceeds co-transcriptionally because large mitoribosomal proteins can form a subcomplex on an unprocessed RNA containing the 16S rRNA. Taken together, our data show that RNA processing links transcription to translation via assembly of the mitoribosome.

INTRODUCTION

The mammalian mitochondrial genome is compact and relatively small, only ~16 kb in size, and encodes 11 mRNAs, as well as two rRNAs and 22 tRNAs required for translation (Figure 1A and reviewed in Rackham et al., 2012). Mammalian mitochondrial mRNAs code for 13 proteins, which are all essential components of the respiratory chain and the ATP synthase that are responsible for energy maintenance by oxidative phosphorylation (OXPHOS). Although the mitochondrial OXPHOS complexes are predominantly composed of polypeptides that are encoded by nuclear genes and imported into mitochondria from the cytosol, their assembly and function is dependent on the expression of the mitochondria-encoded polypeptides (Hällberg and Larsson, 2014). Furthermore, the mitochondrial genome is dependent on nuclear-encoded proteins for replication, repair, transcription, and translation (Hällberg and Larsson, 2014; Rackham et al., 2012). Consequently, the expression of both mitochondrial and nuclear genes requires cooperative regulation to enable balanced energy production. Nuclear gene expression is significantly correlated with mitochondrial gene expression, reflecting close coordination between nuclear and mitochondrial genomes in relation to the energy demands of different tissues (Mercer et al., 2011).

Mitochondrial genes coding for proteins and tRNAs are located on both the heavy and light strands of the mtDNA, which are transcribed as large polycistronic transcripts covering almost the entire length of each strand (Hällberg and Larsson, 2014; Montoya et al., 1981). This differs significantly from nuclear gene transcription and requires several unique processing steps to form functional RNAs. In nearly all cases, genes encoding for protein or rRNA are interspersed by one or more tRNAs, which were proposed to act as "punctuation" marks for processing by Attardi and colleagues (Ojala et al., 1981). This processing involves cleavage at the 5′ end of tRNAs by the RNase P complex (Holzmann et al., 2008; Sanchez et al., 2011) and cleavage of the 3′ ends by the mitochondrial RNase Z (Brzezniak et al., 2011; Sanchez et al., 2011). Processing is followed by maturation of the RNAs, the assembly of the rRNAs into mitochondrial ribosomes, and translation of the mRNAs using tRNAs. Although previously not investigated in vivo, it has been proposed that regulation of the processing of mitochondrial tRNAs might have profound effects on mitochondrial gene expression, the assembly of the protein synthesis machinery, and the overall level of translation, particularly in mitochondrial diseases caused by mutations in regulatory mtDNA-encoded genes such as tRNAs and in mitochondrial RNA-binding proteins that regulate mitochondrial gene expression and are nuclear encoded (Sanchez et al., 2011; Rackham et al., 2012).

In animal mitochondria, the RNase P complex lacks the RNA catalytic component and is composed of only three protein subunits, mitochondrial RNase P protein 1 (MRPP1), MRPP2, and MRPP3 (Holzmann et al., 2008). The MRPP1 subunit of mitochondrial RNase P enzyme has a conserved guanine methyltransferase domain that modifies adenines or guanines at position 9 of mitochondrial tRNAs in addition to its role as a subunit

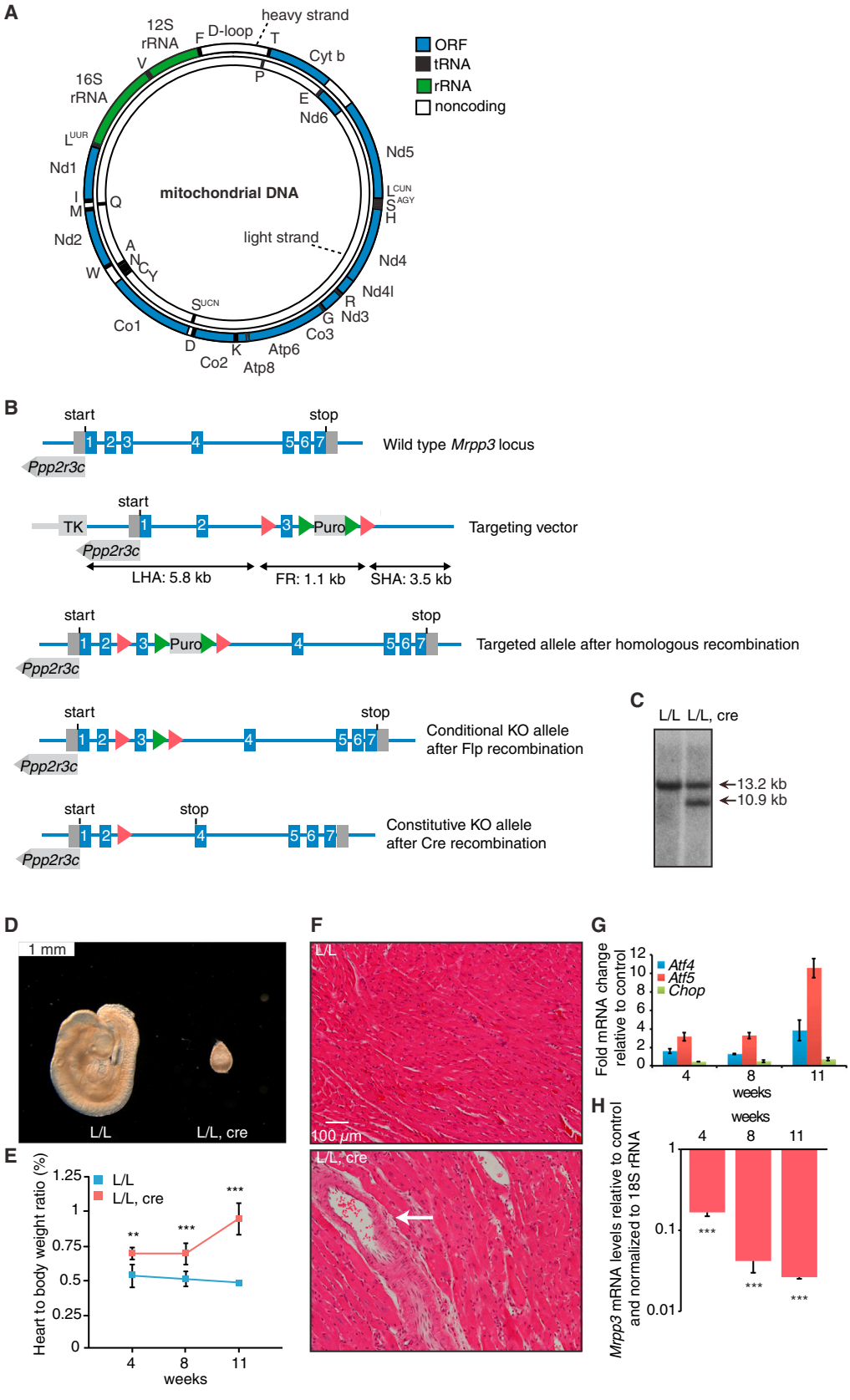

(legend on next page)

of RNase P (Sanchez et al., 2011; Vilardo et al., 2012). MRPP2 is a member of the short-chain dehydrogenase superfamily, and mutations in the gene encoding this protein cause mitochondrial disease as a result of impaired RNA processing, further indicating that it is required for RNase P activity (Vilardo and Rossmanith, 2015; Zschocke, 2012). MRPP3 consists of a metallonuclease domain, which carries out the endonuclease cleavage, and a pentatricopeptide repeat (PPR) RNA-binding domain (Li et al., 2015; Reinhard et al., 2015). The PPR proteins represent a large family of sequence-specific RNA-binding proteins that play a role in organelle gene expression (Small et al., 2013). In mammals, there are only seven PPR domain proteins, all of which are in mitochondria and regulate the different aspects of mitochondrial RNA metabolism from transcription (the mitochondrial RNA polymerase, POLRMT) (Kühl et al., 2014), to processing (PPR domain containing proteins 1 and 2, PTCD1 and PTCD2, mitochondrial RNase P protein 3, MRPP3) (Holzmann et al., 2008; Li et al., 2015; Sanchez et al., 2011; Rackham et al., 2009; Reinhard et al., 2015; Xu et al., 2008), maturation and stability (the leucine-rich PPR cassette protein, LRPPRC) (Ruzzenente et al., 2012; Sasarman et al., 2010), and protein synthesis (the mitochondrial ribosomal protein of the small subunit 27, MRPS27, and PTCD3) (Davies et al., 2012, 2009).

Although in vitro studies have shown that the RNase P complex cleaves mitochondrial tRNAs at their 5′ end (Holzmann et al., 2008; Sanchez et al., 2011), knowledge is lacking about the hierarchy of RNA processing and the consequences of impaired RNA processing on mitochondrial function in vivo. This is particularly important because mutations in the mitochondrial genome that preclude RNA processing at different sites and generate unprocessed transcripts have dire consequences for mitochondrial biogenesis and energy maintenance. Furthermore, we and others have shown that mutations in MRPP1 and MRPP2 lead to severe multi-system disorders and mitochondrial diseases by disruption of 5′ tRNA processing (Metodiev et al., 2016; Zschocke, 2012), and similarly disruption of the 3′ RNA processing as a result of mutations in ELAC2 (the mitochondrial RNaze Z enzyme) causes cardiomyopathy and mitochondrial disease (Haack et al., 2013).

We have generated conditional *Mrpp3* knockout mice and show here that MRPP3 is required for early embryo development and life. Heart- and skeletal-muscle-specific loss of MRPP3 leads to a profound cardiomyopathy and a short lifespan. We show that RNA processing by MRPP3 is required for the biogenesis of the respiratory complexes, their activity, and mitochondrial respiration. Impaired RNA processing precludes the assembly of the ribosomal subunits and thereby the mitochondrial ribosome (mitoribosome). Interestingly, the mitoribosomal proteins are reduced in the absence of a mature rRNA, although a subcomplex of a subset of large ribosomal proteins is able to form on the unprocessed rRNA transcript. Finally, we identify all of the in vivo RNase P cleavage sites and provide a mechanistic link for RNA processing between transcription and protein synthesis.

RESULTS

MRPP3 Is Essential for Development, and Heart-Specific Loss of MRPP3 Causes Cardiomyopathy

MRPP3 shares homology with the proteinaceous RNase P (PRORP) enzymes that lack an RNA catalytic subunit and cleave the 5′ ends of tRNAs in mitochondria, chloroplasts as well as the nucleus of plants and protists (Gobert et al., 2010; Taschner et al., 2012). Despite having an endonuclease domain for the catalytic cleavage of tRNAs, the mitochondrial MRPP3 protein in animal mitochondria requires two additional proteins MRPP1 and MRPP2 for RNase P activity (Holzmann et al., 2008). To understand the in vivo role of MRPP3 in animal mitochondria, we generated a conditional knockout allele of the mouse *Mrpp3* gene by flanking exon 3 with loxP sites in embryonic stem (ES) cells (Figures 1B and 1C) and subsequent transmission through the germline to obtain heterozygous *Mrpp3* $^{+/\text{loxP-puro}}$ animals. These mice were crossed with transgenic mice expressing the Flp recombinase to excise the puromycin cassette (Figure 1B), and the resulting *Mrpp3*$^{+/\text{loxP}}$ mice were mated to mice expressing Cre recombinase under the control of the β-actin promoter to generate heterozygous *Mrpp3* knockout mice (*Mrpp3*$^{+/-}$). Intercrossing the *Mrpp3*$^{+/-}$ mice produced *Mrpp3*$^{+/-}$ and *Mrpp3*$^{+/+}$ mice in Mendelian proportions (genotyped pups n = 115, *Mrpp3*$^{+/-}$ n = 66 and *Mrpp3*$^{+/+}$ n = 49); however, the homozygous knockout mice (*Mrpp3*$^{-/-}$) were not viable. Previous analyses of essential proteins involved in mitochondrial gene expression have observed embryonic lethality at E8.5 (Cámara et al., 2011; Larsson et al., 1998; Metodiev et al., 2009, 2014; Park et al., 2007; Ruzzenente et al., 2012); therefore, we analyzed the embryos at this stage to identify that *Mrpp3*$^{-/-}$ embryos had not developed normally compared to those observed for *Mrpp3*$^{+/+}$ and *Mrpp3*$^{+/-}$ mice, and hence the loss of MRPP3 was embryonic lethal (Figure 1D). Based on these findings, we conclude that MRPP3 is essential for embryo development and survival.

Figure 1. Full-Body Knockout of MRPP3 Causes Embryonic Lethality and Cardiomyopathy in Heart-Specific Knockout Mice

(A) Schematic representation of the gene organization in mammalian mtDNA.

(B) Schematic showing the disruption of the *Mrpp3* gene (also known as *1110008LRik* and *Kiaa0391*). LoxP sites flanking exon 3 of the *Mrpp3* gene were inserted in the mouse genome by homologous recombination. The long homology arm (LHA), floxed regions (FR), and short homology arm (SHA) are shown.

(C) Homologous recombination at the *Mrpp3* locus shown by Southern blotting.

(D) Morphology of the *Mrpp3*$^{+/+}$ and *Mrpp3*$^{-/-}$ embryos at day E8.5. Scale bar, 1 mm.

(E) Heart weight to body weight ratio in control (L/L) and knockout mice (L/L, cre) at different ages. At 4 weeks, L/L n = 8, L/L, cre n = 8; at 8 weeks, L/L n = 12, L/L, cre n = 12; at 11 weeks, L/L n = 12, L/L, cre n = 12. Error bars, SEM; **p < 0.01; ***p < 0.001, Student's t test.

(F) H&E, NADH, and COX and trichrome gomorii staining of hearts from control (L/L) and knockout mice (L/L, cre).

(G) Levels of *Atf4*, *Atf5*, and *Chop* mRNAs were determined in isolated total heart RNA from control (L/L) and knockout mice (L/L, cre) by qRT-PCR (n = 5). The data are expressed relative to control mice and normalized to 18S rRNA.

(H) *Mrpp3* transcript levels were determined in isolated total heart RNA from control (L/L) and knockout mice (L/L, cre) by qRT-PCR (n = 5). The data are expressed relative to control mice and normalized to 18S rRNA.

Next, we crossed *Mrpp3*$^{+/loxP}$ mice with transgenic mice expressing a Cre recombinase under the control of muscle creatinine kinase promoter (*Ckmm-cre*) to produce heart- and skeletal-muscle-specific *Mrpp3* knockout mice (*Mrpp3*$^{loxP/loxP,\ +/}$*Ckmm-cre*). The MRPP3 mice with *Ckmm-cre*-directed knockout have a short lifespan and die by 11 weeks of cardiomyopathy, determined by the increased size of the heart, by measuring the heart weight to body weight ratio (Figure 1E) and by histology, indicating the accumulation of necrotic foci in the myocardium of these mice (Figure 1F). Furthermore, we observed that the transcription factors ATF4 and ATF5, that are elevated in cardiomyopathy as a result of mitochondrial dysfunction (Dogan et al., 2014), are significantly increased in the *Mrpp3* knockout mice compared to their age and sex matched controls (*Mrpp3*$^{loxP/loxP}$), and this increase is most apparent at 11 weeks (Figure 1G). These physiological changes in the knockout mice are a consequence of the *Mrpp3* deletion and loss of *Mrpp3* expression measured by qRT-PCR over 4, 8, and 11 weeks (Figure 1H). We confirmed that loss of *Mrpp3* expression in skeletal muscle over the same time (Figure S1A) resulted in reduced muscle fiber appearance and reduction in complex I and complex IV staining (Figure S1B), without any effects on ATF4 and ATF5 expression (Figure S1C), indicating that cardiomyopathy is the major cause of death in these mice.

Defects in RNA Processing Increase the Rate of Transcription and Impair Protein Synthesis

We investigated the effects of MRPP3 loss on mitochondrial transcription by de novo pulse and chase labeling with ^{32}P/radiolabeled uridine triphosphate (UTP) and identified that impaired tRNA 5′ end processing led to a significantly increased rate of transcription relative to controls (Figure 2A). It is interesting that the mature 12S and 16S rRNA bands that most prominently featured in the controls are not observed in the *Mrpp3* knockout mice, and instead we observe higher molecular weight unprocessed transcripts in these mice (Figure S2A). Northern blotting of these membranes confirmed that mitochondrial mRNAs, tRNAs, and rRNAs are contained within the higher molecular weight bands in the *Mrpp3* knockout mice and that there are no mature transcripts produced in these mice compared to controls (Figure S2B). In contrast, de novo mitochondrial translation measured using ^{35}S-methionine and cysteine incorporation revealed significant reduction in protein synthesis of all mitochondrially encoded proteins in the *Mrpp3* knockout mice compared to controls (Figure 2B). Immunoblotting of mtDNA- and nuclear-encoded polypeptide components of the electron translocating respiratory complexes revealed a significant decrease in their levels that is most pronounced at 11 weeks in the *Mrpp3* knockout mice (Figure 2C). The two subunits of the ATP synthase, ATP5A and ATP8, were present at near normal levels. Loss of MRPP3 did not affect the levels of the complex II subunit SDHB (Figure 2C), indicating that the reduction of the nuclear-encoded subunits of the other respiratory complexes was a consequence of the decreased levels of the mitochondria-encoded respiratory polypeptides that form the same complexes. This indicates that loss of mitochondrial tRNA 5′ end processing affects the biogenesis of the electron translocating respiratory complexes and is rate limiting for their formation. Furthermore, we show that increased transcription is not sufficient to overcome the inability to process the newly produced transcripts.

MRPP3 Is Required for Mitochondrial Respiratory Complex Biogenesis and Function

We investigated the effects of MRPP3 loss on the abundance and integrity of the mitochondrial respiratory complexes by blue native (BN)-PAGE (BN-PAGE). We observed decreased abundance of all proton translocating respiratory complexes in the *Mrpp3* knockout mice, but not in the control mice (Figure 2D). In addition, we measured the in-gel activities of complexes I and IV and show that they are dramatically reduced in the *Mrpp3* knockout mice relative to controls (Figure 2D). Loss of MRPP3 results in significant reduction of respiratory supercomplexes as a result of their decreased biogenesis and stability (Figures 2D). The reduced levels of the respiratory complexes in the *Mrpp3* knockout mice were confirmed by immunoblotting following BN-PAGE and confirmed that the levels of complex II are slightly increased (Figure S2C).

Next, we determined the consequences of MRPP3 loss on mitochondrial function by measuring the activities of respiratory complexes in control and *Mrpp3* knockout mice (Figures 2E and 2F). The activities of complexes I, III, and IV were all significantly decreased in the *Mrpp3* knockout mice, consistent with their decreased levels observed on BN-PAGE and immunoblotting (Figures 2D and S2C). Complex II activity was slightly increased (Figure 2E), which is typically observed when there is a general oxidative phosphorylation (OXPHOS) defect (Duff et al., 2015). Measurement of mitochondrial oxygen consumption showed that there was a significant reduction in the non-phosphorylated, phosphorylated, and uncoupled respiration state in the *Mrpp3* knockout mice (Figure 2F). Therefore, loss of MRPP3 causes profound mitochondrial dysfunction by causing general OXPHOS defects, further indicating that RNA processing is essential for mitochondrial function.

The Mitochondrial RNase P Regulates the Processing of Canonical tRNA 5′ Ends

MRPP3 has been shown to cleave the 5′ ends of mitochondrial tRNAs when it is part of the RNase P complex with MRPP1 and MRPP2 in vitro (Holzmann et al., 2008; Li et al., 2015; Reinhard et al., 2015). We have shown that the mitochondrial RNase P cleaves the 5′ ends of mitochondrial tRNAs and can have promiscuous activity toward RNAs that have tRNA-like structures at their 5′ ends in cells (Sanchez et al., 2011). However, all of these effects have been investigated in cells grown in high glucose where the *MRPP3* levels have been knocked down and given the high stability of the protein it is necessary to investigate the effects of MRPP3 loss in vivo. Furthermore the hierarchy of RNA processing has not been investigated previously; therefore, we analyzed the effects of the MRPP3 loss on the order of cleavage and abundance of steady-state mitochondrial RNAs in hearts by northern blotting over 4, 8, and 11 weeks.

MRPP3 loss leads to gradual loss of mature mRNAs such as *mt-Co1*, *mt-Nd1*, *mt-Atp8/6*, and *mt-Cyt b* by 11 weeks and a converse increase in the accumulation of unprocessed and precursor transcripts (Figure 3A). In contrast, the mature *mt-Nd5*

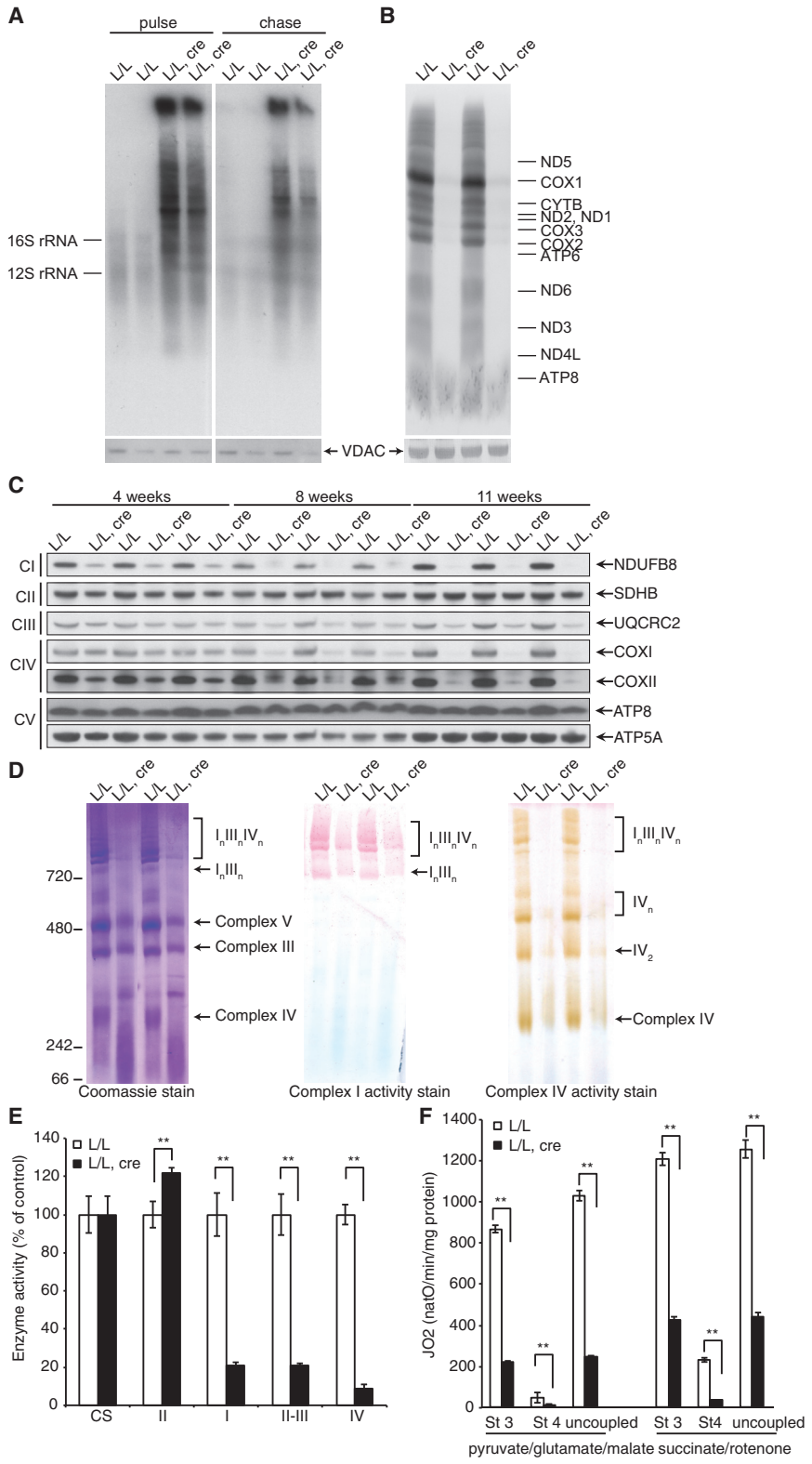

Figure 2. Loss of MRPP3 Impairs Mitochondrial Biogenesis and Increases Transcription

(A) In organello transcription was measured in heart mitochondria in the presence of ^{32}P-labeled UTP, and the radiolabeled RNA was isolated and resolved on a 0.9% formaldehyde gel that was visualized by autoradiography. VDAC was used as a loading control. The data are representative of results obtained for 11-week-old L/L and L/L, cre mice (n = 6) in three independent biological experiments.

(B) Protein synthesis in heart mitochondria from 11-week-old control and knockout mice was measured by pulse incorporation of ^{35}S-labeled methionine and cysteine. Equal amounts of mitochondrial protein (50 μg) were separated by SDS-PAGE, immunoblotted for VDAC to show equal loading and visualized by autoradiography. Representative gels are shown of three independent biological experiments.

(C) Mitochondrial proteins (25 μg) from 4-, 8-, and 11-week-old heart mitochondria from control and knockout mice were resolved on 4%–20% SDS-PAGE gels and immunoblotted against antibodies to investigate the steady-state levels of nuclear and mitochondrial-encoded proteins. ATP5A was used as a loading control.

(D) Heart mitochondria (75 μg) treated with 1% digitonin were separated on a 4%–30% BN-PAGE, and the respiratory complexes were visualized by Coomassie staining. In-gel activity stains were used for complex I and complex IV.

(E) Respiratory complex activities were measured spectrophotometrically and normalized to citrate synthase activity in mitochondria isolated from hearts of 11-week-old control and knockout mice (n = 6). Error bars, SEM; **p < 0.01; ***p < 0.001, Student's t test.

(F) Loss of the MRPP3 causes profound reduction in mitochondrial respiration at complex I, II-III, and IV in the KO mice compared to controls. Non-phosphorylating (state 4), phosphorylating (state 3), and uncoupled respiration in the presence of 0.5 μM carbonyl cyanide 3-chlorophenylhydrazone (CCCP) was measured in heart mitochondria using an Oroboros oxygen electrode using pyruvate, glutamate and malate, or succinate as a substrates in the presence of rotenone as indicated. Error bars, SEM; **p < 0.01; ***p < 0.001, Student's t test.

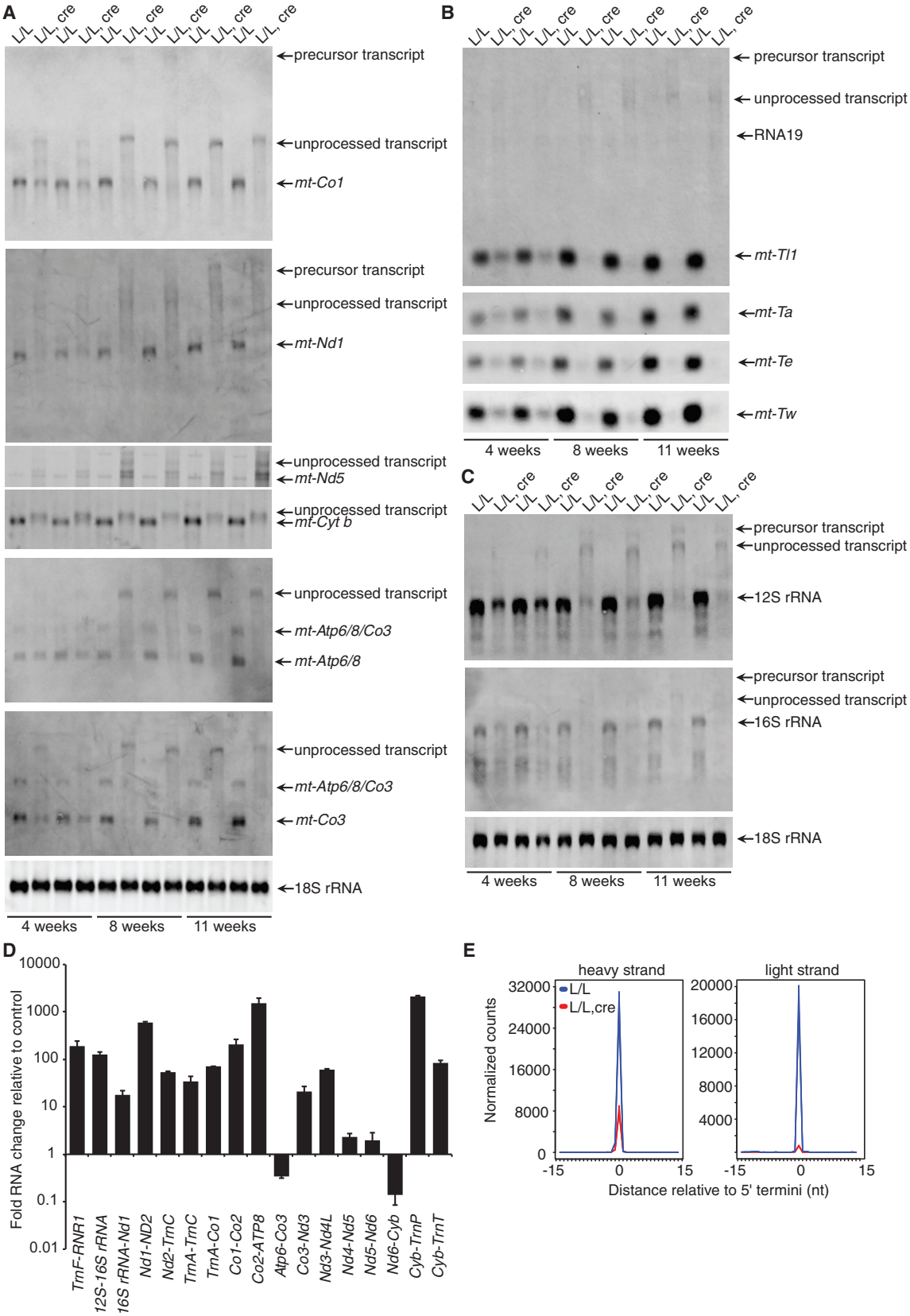

(legend on next page)

levels are not dramatically affected by the loss of MRPP3 (Figure 3A), which is likely a consequence of its organization within the mitochondrial genome (Figure 1A). The 3′ end of $tRNA^{Leu(CUN)}$ is in effect the 5′ end of *mt-Nd5* that is cleaved by the mitochondrial RNase Z or ELAC2 along with its 3′ end, thereby allowing it to be produced as a correctly processed mature mRNA. The 3′ end of *mt-Nd5* is a "mirror tRNA" of $tRNA^{Glu}$, which must be processed by either ELAC2 or another endonuclease because it seems to be unaffected by the loss of MRPP3. MRPP3 loss also leads to lack of mature tRNAs as a consequence of their accumulation within unprocessed transcripts (Figure 3B). The levels of the mature mitochondrial rRNAs are significantly decreased, whereas unprocessed transcripts accumulate in the *Mrpp3* knockout mice relative to controls (Figure 3C). It is interesting to note that the organization of the 12S and 16S rRNAs should allow them to be processed by the RNase Z at the 3′ ends thereby leaving them with $tRNA^{Val}$ and $tRNA^{Leu(UUR)}$ attached at their 5′ ends, respectively. However, instead we observe loss of each 12S and 16S rRNA by 11 weeks (Figure 3C) providing the first experimental evidence that 3′ tRNA processing is dependent on functional 5′ tRNA processing to release the rRNAs.

We used qRT-PCR to investigate processing events across every canonical junction in the mitochondrial transcriptome (Figure 3D) and to account for any junctions that are not processed by the RNase P complex that was not possible to assess by northern blotting because of the organization of the genome (Figure 1A) and the hierarchical RNA processing. There was significant accumulation of precursors in the *Mrpp3* knockout mice compared to controls. The magnitude of changes in these precursors indicates the stabilities of their unprocessed forms as well as the efficiency of normal processing at these junctions (Figure 3D). For example the *mt-Cyt b-*$tRNA^{Pro}$ precursor was the most abundant and likely most stable, compared to the *mtNd4-mtNd5* and *mtNd5-mtNd6* precursors that were least abundant because of the multiple ELAC2 sites that span *mtNd4-mtNd5* and that *mtNd5-mtncNd6* does not require MRPP3 for processing (Figure 3D). Interestingly, because the qRT-PCR examined individual junctions we were able to identify two sites, between the *mt-ATP8/6* and *mt-Co3* and the 5′ end of *mt-Nd6*, that are not cleaved by RNase P. We have shown previously that the 5′ end of *mt-Nd6* is produced by cleavage at the 3′ end of $tRNA^{Glu}$ by the RNase Z, ELAC2 (Sanchez et al., 2011), and FASTKD5 affects the processing of the *mt-ATP8/6* and *mt-Co3* precursor, commonly known as *RNA14* (Antonicka and Shoubridge, 2015). We identified a similar increase in junction accumulation in skeletal muscle (Figure S2D), identifying that mitochondrial dysfunction (Figures S1A–S1C) was a result of impaired RNA processing due to loss of MRPP3 in this tissue.

RNase P Processing Precedes 3′ tRNA Cleavage

We used parallel analyses of RNA ends (PARE) (German et al., 2009; Mercer et al., 2011; Rackham and Filipovska, 2014a) to investigate the distribution of 5′ ends across the entire mitochondrial transcriptome from three control and three knockout mice, respectively, and identify the 5′ canonical, and any previously unknown sites, that are processed by MRPP3 (Figure 3E) and account for cleavage sites that are a result of other processing enzymes (Figure 4A; Table S1). PARE captures ~20-nt tags from the 5′ ends of 5′-monophosphorylated RNAs and the normalized read count at the 5′ terminal positions accumulate at canonical and abundant processing sites to form identifiable peaks, whose relative change between control and knockout mice reveals sites of impaired processing upon the loss of MRPP3 (i.e., Figure 4B). We found a dramatic reduction in reads mapping to the annotated 5′ ends of transcripts derived from both the heavy and light strands of the mitochondrial genome (Figure 3E), confirming that MRPP3 is critical for their processing. We present a transcriptome-wide map of 5′ end processing sites (Figures 4A and S3A) that identified and confirmed the canonical cleavage sites detected by qRT-PCR (Figure 3D). Furthermore PARE identified that 5′ end cleavage precedes 3′ processing by the mitochondrial RNase Z enzyme ELAC2 because we observe a dramatic decrease in processing at the 5′ ends of mt-mRNAs that border the 3′ ends of the adjacent tRNA, which should be substrates for ELAC2. For example, there is a marked decrease in cleavage at the 5′ end of 16S rRNA, which borders the 3′ end of mt-$tRNA^{Val}$ (Figure 4B); we found the same consistent reduction in the processing of the 5′ end of *mt-Nd1* mRNA, which borders the 3′ end of mt-$tRNA^{Leu(UUR)}$ (Figure 4C) and a reduction in the 5′ end of *mt-Nd2* mRNA, which borders the 3′ end of mt-$tRNA^{Met}$ (Figure S3B). We confirmed our PARE findings further by transcriptome-wide RNA sequencing (RNA-seq) of three control and three knockout mice (Figure 4A) where, unlike for PARE, these libraries captured longer reads across the entire mitochondrial transcriptome and excluded short RNAs, such as tRNAs. Consequently, this technique captures tRNAs that are part of unprocessed transcripts and by analyzing reads that span processed regions in the mitochondrial transcriptome we quantified regions that are increased in the MRPP3 knockout mice where processing is impaired. Therefore, regions between processing sites where processing is impaired should have an increased abundance of reads in RNA-seq datasets but reduced processing events, peaks, in PARE datasets. In our RNA-seq datasets, we found an enrichment of reads across junctions that span tRNA regions between the mRNA and rRNA genes, indicating an increase in precursor RNAs. In support of this, we observe a concomitant reduction in mature mtRNAs as a result of the accumulation of the polycistronic precursor mtRNAs on northern

Figure 3. Loss of MRPP3 Causes Impaired RNA Processing

(A–C) The abundance of mature mitochondrial mRNAs (A), tRNAs (B), and rRNAs (C) in hearts from 4-, 8-, and 11-week-old control and knockout mice were analyzed by northern blotting. 18S rRNA was used as a loading control. The data are representative of results obtained from at least eight mice from each strain and three independent biological experiments.

(D) The canonical mitochondrial RNA junctions were measured in total heart RNA from control (L/L) and knockout (L/L, cre) mice by qRT-PCR and normalized to 18S rRNA. Error bars, SEM; $^{**}p < 0.01$; $^{***}p < 0.001$, Student's t test.

(E) Frequency distribution of PARE reads from heart mitochondrial RNA from three control (L/L; blue) and three knockout (L/L, cre; red) mice. Windows are centered on reads that align 15 nt away from either side of all annotated 5′ ends of mitochondrial tRNAs from the heavy and light chain.

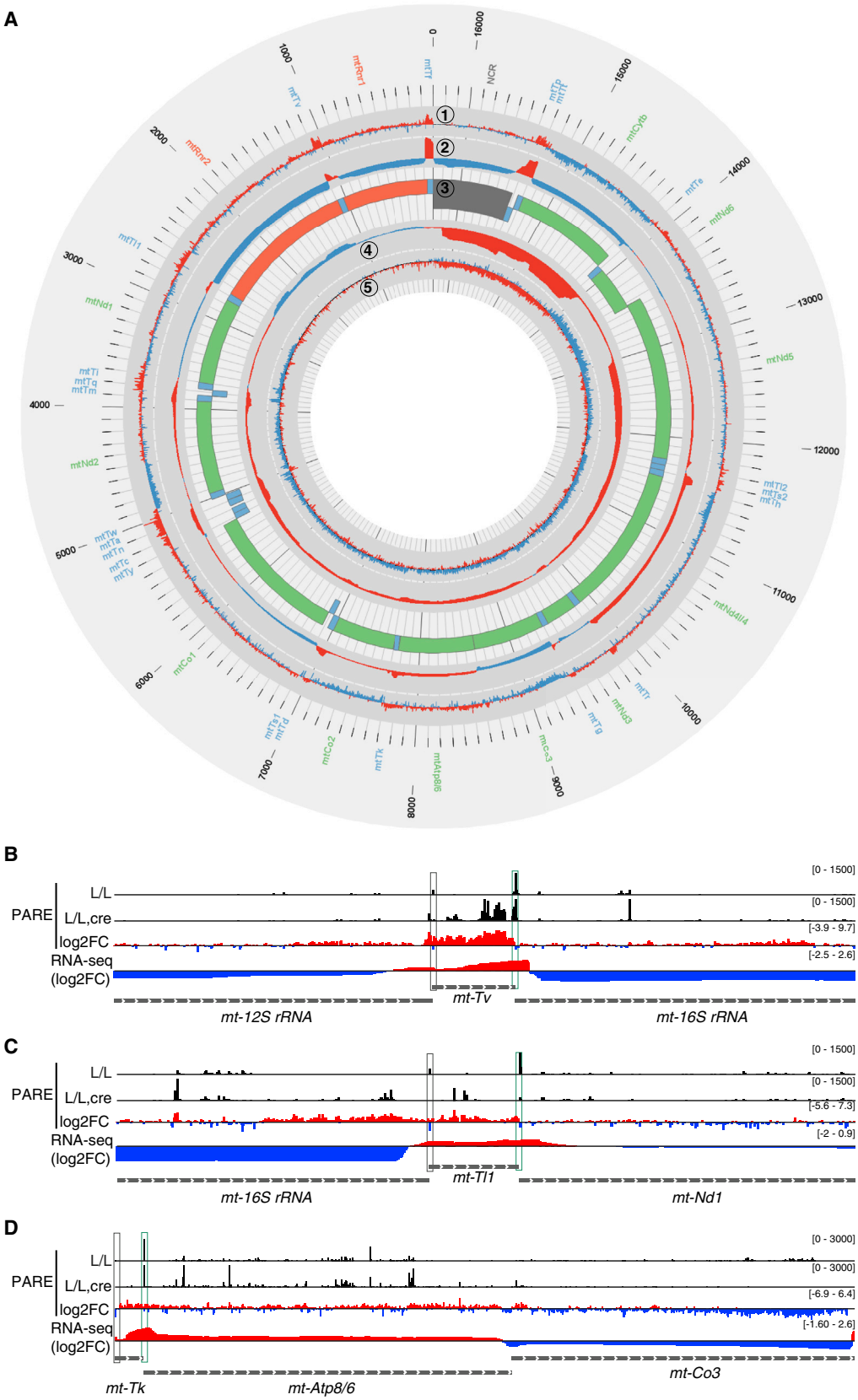

(legend on next page)

blots (Figures 3A–3C). The accumulation of precursor transcripts shown by RNA-seq correlates well with the decrease or loss of 5′ and 3′ ends found with the PARE data as well as the northern blots indicating that there is a hierarchy of mtRNA processing where 5′ end processing is the initial step in vivo.

Although we found a decrease in 3′ end processing, we observed at least one instance where ELAC2 activity was not affected or increased by the lack of 5′ processing, such as at the 3′ end of *tRNA^{Lys}*, which borders the 5′ end of *mt-Atp8/6* (Figure 4D). This effect might be due to the increased stability or abundance of these RNAs in the absence of RNase P processing as indicated by the increased levels of this precursor transcript in our qRT-PCR data (Figure 3D). Interestingly, we identified two sites where the ELAC2 activity is increased in the knockout mice in a region containing multiple tRNAs encoded by both the heavy and light strand (Figure S3C). We find that the 3′ ends of both heavy-strand-encoded *tRNA^{Ile}* and *tRNA^{Trp}* are increased (Figure S3C), even though the 3′ ends of their respective light-strand-encoded *tRNA^{Gln}* and *tRNA^{Ala}* are decreased, which may be due to altered structures of these regions when flanking RNA sequences are not removed or heavy strand "mirror tRNA" structures that are recognized by ELAC2 and cleaved. We observe an increased "mirror" *tRNA^{Tyr}* cleavage on the heavy strand in the knockout mice (Figure S4A), the same site that was recently identified three nucleotides upstream of the annotated 5′ of the *mt-Co1* mRNA (Okui et al., 2016), suggesting that this site is cleaved independently of MRPP3.

We identified a site between the *mt-Atp8/6* and *mt-Co3* mRNAs that is not covered in our PARE datasets (Figure 4D). The absence of this 5′ end suggests that this site may not contain a 5′ phosphate as it is required for PARE and it may be processed by an entirely different mechanism. In addition, in RNA-seq coverage we find a dramatic change at the junction between *mt-Atp8/6* and *mt-Co3* in the knockout mice, suggesting that ELAC2 or another endonuclease such as FASTKD5 (Antonicka and Shoubridge, 2015) may be able to preferentially cleave around this site in the absence of MRPP3.

In the PARE data from the knockout mice, we observed an increased number of free 5′ ends across the entire lengths of transcripts, which was indicative of degradation, most likely of the precursor transcripts that accumulate as a result of impaired processing and increased transcription, which produces a high load of unprocessed RNAs within mitochondria (Figure 4A). This was also apparent in the significant reduction of mature mtRNAs in the RNA-seq datasets (Figure 4A) as well as those found by northern blotting (Figures 3A–3C). We investigated the specificity of mtRNA degradation digitally by searching for motifs around the cleavage sites that are enriched in the absence of MRPP3 and correlating it to the abundance of each nucleotide in the heavy and light strand of the mouse mitochondrial transcriptome (Figure S4B). We conclude that the degradation is carried out by an endonuclease that lacks sequence specificity.

Mitochondrial RNA Processing Is Required for the Assembly of the Mitoribosome and the Stability of Ribosomal Proteins

To investigate the changes in gene expression as a result of MRPP3 loss, we carried out transcriptome-wide RNA-seq and identified the most significant effects on heart and mitochondrial function (Figure 5A). We observed a significant decrease of cardiac markers such as cardiac actin and myosins as well as the ryanodine receptor 2 (Figure 5A; Table S2), consistent with the development of cardiomyopathy (Figures 1D and 1F). Transcripts encoding mitochondrial proteins, particularly those encoding the electron transport chain polypeptides, were most changed in response to MRPP3 loss and consequent mitochondrial dysfunction (Figure 5A; Table S2). Also, transcripts involved in translation were significantly affected, and those involved in mitochondrial translation were reduced, whereas transcripts involved in cytosolic translation were increased, likely as a way to stimulate mitochondrial biogenesis and compensate for dysfunctional energy metabolism (Figure 5B). We investigated the effects of MRPP3 loss on the mRNAs encoding mitochondrial ribosomal proteins and identified that their levels were largely reduced (Figure 5B), consistent with the loss of mitochondrial translation (Figure 2B).

Mitochondrial gene expression is predominantly regulated at the post-transcriptional level by RNA-binding proteins (Liu et al., 2013). Therefore, to investigate the consequences of impaired tRNA 5′ end processing over 4, 8, and 11 weeks and validate our RNA-seq data, we analyzed the effects of MRPP3 loss on nuclear-encoded mitochondrial RNA-binding proteins

Figure 4. Transcriptome-wide Analyses of 5′ tRNA Cleavage Sites by PARE and RNA-Seq

(A) A complete map of changes in 5′ end abundance (1, 5; $\log_2$ fold change[KO_{mean}/$Ctrl_{mean}$]) and RNA-seq coverage (2, 4; $\log_2$ fold change[KO_{mean}/$Ctrl_{mean}$]) from three control (L/L) and three knockout (L/L, cre) mice, on heavy (1, 2) and light (4, 5) strands. Increases are shown in red and decreases in blue. The mitochondrial genome is displayed in the central track (3), with the nucleotide position in base pairs displayed across the exterior; rRNAs are displayed in orange, mRNAs in green, tRNAs in blue, and the non-coding region (NCR) in gray.

(B) Genome browser view of the 5′ end abundance from three control (L/L) and three knockout (L/L, cre) mice (top; mean normalized count), and relative changes in mean 5′ end abundance (middle; $\log_2$ fold change[KO_{mean}/$Ctrl_{mean}$]), and mean RNA-seq coverage (bottom; $\log_2$ fold change[KO_{mean}/$Ctrl_{mean}$]) showing the 5′ cleavage sites of *mt-tRNA^{Val}* by MRPP3 and the downstream effect on the 3′ end of the *12S* rRNA in the absence of MRPP3. Regions of interests are shown in gray (for 5′ ends) and green (for 3′ ends) boxes.

(C) Genome browser view of the 5′ end abundance from three control (L/L) and three knockout (L/L, cre) mice (top; mean normalized count), and relative changes in mean 5′ end abundance (middle; $\log_2$[KO_{mean}/$Ctrl_{mean}$]), and mean RNA-seq coverage (bottom; $\log_2$[KO_{mean}/$Ctrl_{mean}$]) showing the 5′ cleavage sites of *mt-tRNA$^{Leu(UUR)}$* by MRPP3 and the downstream effect on the 3′ end of the *mt-Nd1* mRNA in the absence of MRPP3. Regions of interests are shown in gray (for 5′ ends) and green (for 3′ ends) boxes.

(D) Genome browser view of the 5′ end abundance from three control (L/L) and three knockout (L/L, cre) mice (top; mean normalized count), and relative changes in mean 5′ end abundance (middle; $\log_2$ fold change[KO_{mean}/$Ctrl_{mean}$]), and mean RNA-seq coverage (bottom; $\log_2$ fold change[KO_{mean}/$Ctrl_{mean}$]) showing the non-canonical region between *mt-Atp8/6* and *mt-Co3* and the 5′ cleavage sites of *mt-tRNA^{Lys}* by MRPP3 and the lack of effect on the 3′ end of the *mt-Atp8/6* mRNA in the absence of MRPP3. Regions of interests are shown in gray (for 5′ ends) and green (for 3′ ends) boxes.

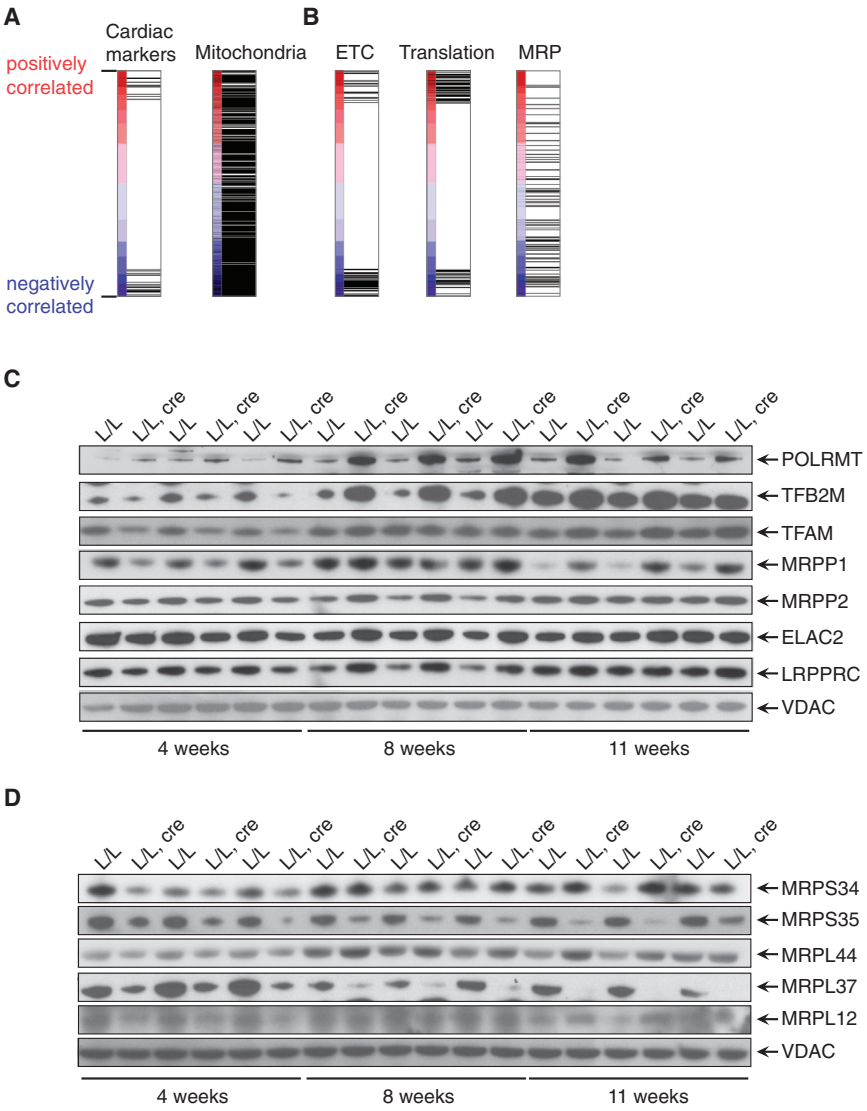

Figure 5. Impaired RNA Processing Causes an Imbalance in Nuclear-Encoded Mitochondrial Proteins

Transcriptome-wide RNA-seq was carried out on total heart RNA from three control (L/L) and three knockout (L/L, cre) mice, and differential expression analyses were performed.

(A and B) Significant differences ($p < 0.05$) in positively and negatively correlated transcripts relative to controls are based on specific gene ontologies are shown for cardiac markers and mitochondrial genes (A) and for oxidative phosphorylation, the translation machinery, and mitoribosomal and RNA-binding proteins (B).

(C) The levels of nuclear-encoded mitochondrial RNA-binding proteins were measured by immunoblotting in heart mitochondria from 4-, 8-, and 11-week-old control (L/L) and knockout (L/L, cre) mice.

(D) Mitochondrial ribosomal protein abundance was measured by immunoblotting in heart mitochondria from 4-, 8-, and 11-week-old L/L and L/L, cre mice.

by immunoblotting. We found that the increased rate of transcription in the *Mrpp3* knockout mice (Figure 2A) was a consequence of increased POLRMT levels as a retrograde response of nuclear gene expression to impaired mitochondrial tRNA processing (Figure 5C). Similarly, we observed increased levels of the two mitochondrial transcription factors, TFAM and TFB2M, in *Mrpp3* knockout mice at 8 and 11 weeks of age (Figure 5C). The levels of the other two RNase P proteins, MRPP1 and MRPP2, were also increased, as well as those of ELAC2 (Figure 5C), likely to compensate for the loss of MRPP3. Interestingly, the LRPPRC protein, required for the stability and translation of mt-mRNAs, is also increased at weeks 8 and 11, possibly as a consequence of the low levels of mature mRNAs. The levels of POLRMT are consistently increased from 4 to 11 weeks in contrast to the other mitochondrial RNA-binding proteins that show an initial decrease in their levels at week 4 in the *Mrpp3* knockout mice but increase their levels relative to controls by weeks 8 and 11 (Figure 5C). This suggests that the initial compensatory response to impaired RNA processing is to increase the rate of transcription, which has also been observed upon knockout of mitochondrial RNA-binding proteins that affect the stability of the ribosome such as TFB1M, MTERF3, and MTERF4 (Cámara et al., 2011; Metodiev et al., 2009; Park et al., 2007). This is in contrast to other proteins that regulate mitochondrial gene expression, such as LRPPRC, where the rate of transcription is not affected (Ruzzenente et al., 2012).

Since mitochondrial protein synthesis was significantly reduced in the *Mrpp3* knockout mice, we investigated the effects of MRPP3 loss on the steady-state levels of mitoribosomal proteins (Figure 5D). We found that the levels of some ribosomal proteins were increased in the *Mrpp3* knockout mice, such as MRPS34 and MRPL12, whereas some were decreased such as MRPS35 and MRPL37 (Figure 5D), consistent with the differential expression and enrichment analyses of the mRNAs encoding mitoribosomal proteins found in our RNA-seq data (Figure 5A; Table S2). These findings indicate that impaired tRNA processing affects mitoribosome stability, as we have observed before in cells (Sanchez et al., 2011).

To investigate the effects of impaired tRNA processing on the assembly and stability of the ribosome, we resolved the mitoribosomal subunits and assembled ribosomes on 10%–30% sucrose gradients and examined them by immunoblotting against markers of the small and large ribosomal subunits (Figure 6A). We identify that loss of MRPP3 and hence tRNA 5′ end processing impairs 55S monosome formation (Figure 6A). Furthermore, we observed a shift of the small and large ribosomal subunit proteins toward the less dense sucrose fraction in the *Mrpp3*

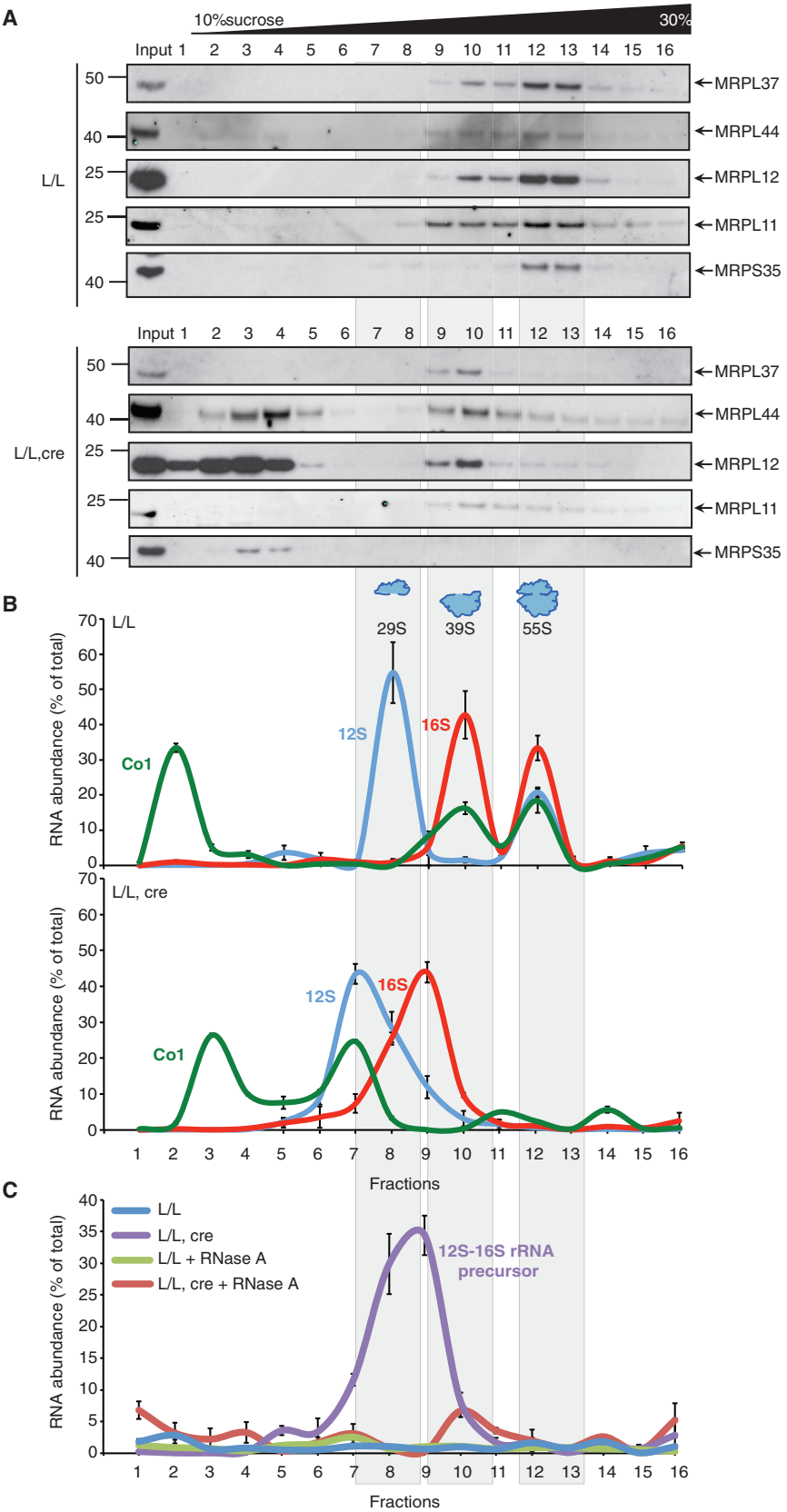

Figure 6. Mitochondrial Ribosome Assembly Is Impaired as a Consequence of Impaired RNA Processing

(A) A continuous 10%–30% sucrose gradient was used to determine the distribution of the small and large ribosomal subunit and the monosome in the control and knockout mice. Mitochondrial ribosomal protein markers of the small (MRPS35) and large (MRPL37, MRPL44, MRPL11, and MRPL12) ribosomal subunits were detected by immunoblotting with specific antibodies. The input (10% of the total lysate) was used as a positive control. The data are representative of results from at least three independent biological experiments.

(B and C) The distribution of the *mt-Co1* mRNA, *12S* and *16S* rRNAs (B), and *12S-16S* rRNA junctions (C) in sucrose gradients were analyzed by qRT-PCR. The data are expressed as percentage of total RNA abundance and are representative of results from four independent biological experiments.

knockout mice compared to controls (Figure 6A). The shift in small ribosomal subunit proteins was dramatic, indicating that the assembly of these proteins on unprocessed 12S rRNA is not possible or at least severely impaired. In contrast, the large ribosomal subunit proteins were shifted but still migrated in a large molecular weight complex, suggesting that a partial ribosomal subcomplex is formed. It is possible that an unprocessed rRNA transcript may be sufficient to stimulate the assembly of the early assembling ribosomal proteins that form a subcomplex but are unable to complete the assembly of the mature subunits. Interestingly, the MRPL37 and MRPL11 proteins, whose abundance was decreased like most mitoribosomal proteins examined, were only found in this subcomplex, while MRPL12, whose abundance was increased in the knockout (Figure 5D), and MRPL44, were found both in the subcomplex and in a rRNA free state in the less dense fractions. This indicates that some ribosomal proteins are stable when unassembled, while others are not. Whether free mitoribosomal proteins might contribute to mitochondrial dysfunction is not known.

Next, we investigated the distribution of mitochondrial transcripts within the ribosomal fractions by qRT-PCR of each fraction (Figure 6B) to determine the distribution of the unprocessed transcripts within the sucrose gradient in the control mice. The distribution of the 12S and 16S rRNA follows a similar pattern as that observed by immunoblotting against markers of the small and large ribosomal subunits, respectively (Figure 6B). However, we observe a redistribution of these transcripts in the *Mrpp3* knockout mice to less dense fractions of the sucrose gradient (Figure 6B) that co-migrate with the unprocessed polycistronic transcripts that contain both the 12S and 16S rRNAs (Figure 6C). Similarly, we observe that the *mt-Co1* mRNA is present in the pool of free mt-mRNAs in the top fractions as well as with the ribosomal fractions in the control mice; however, it is re-distributed only to the earlier fractions in the *Mrpp3* knockout mice because there are no correctly assembled mitoribosome subunits to recruit mRNAs (Figure 6B). We find that the *mt-tRNA*$^{Leu(UUR)}$ is not present in its mature form, but instead it is also part of the large unprocessed transcript found in the *Mrpp3* knockout mice (Figure S4C). We do not observe a polycistronic transcript in the control mice, indicating that the unprocessed transcript that co-migrates with the large subcomplex detected in the immunoblots *Mrpp3* knockout mice (Figure 6A) is composed of ribosomal proteins that assemble on the unprocessed transcript containing the 12S and 16S rRNA. RNase A treatment of mitochondrial lysates before sucrose gradient separation (Figure 6C) identified that the precursor transcript is lost upon RNase treatment, as this transcript is not protected it is likely that it is not bound by a complete complement of mitoribosomal proteins.

To identify the ribosomal proteins that are present in the subcomplex found in fraction 10 on the precursor transcript, we carried out proteomic analyses on fractions that contained the small (fraction 8) and large subunit (fraction 10) or the subcomplex (fraction 8 and 10) and the monosome (fractions 12 and 13) from both the control and *Mrpp3* knockout mice (Figure 7). We confirmed that the monosome is not formed in the *Mrpp3* knockout mice, compared to the control mice where we find the highest abundance of both small and large ribosomal proteins in the monosome fractions (Figure 7). In control mice, the distribution of the small and large subunits is consistent with their migration in the gradient, where the small and large ribosomal subunit proteins are found in the fractions containing the monosome (fractions 12 and 13). In the *Mrpp3* knockout mice, we find enrichment of large ribosomal proteins in fraction 10 indicating that these proteins assemble on the unprocessed transcript to form the subcomplex observed by immunoblotting (Figure 6A). Furthermore, as we detected an enrichment of the majority of large subunit proteins in fraction 10, this complex must be stalled close to the end of the large subunit assembly pathway. Taken together, we have shown that RNA processing is rate limiting for the assembly of the mitochondrial ribosomal subunits and the 55S monosome.

DISCUSSION

The compact organization of the mitochondrial genome in animals has eliminated the necessity for RNA splicing of non-coding inter- and intragenic sequences. Instead, the tRNA genes separate the mRNAs and rRNAs in a way that permits the tRNA endoribonucleases to cleave them from the large polycistronic transcripts produced by the mitochondrial RNA polymerase and release all individual mtRNAs (Ojala et al., 1981). Although two enzymes involved in 5′ and 3′ tRNA processing have been identified as the RNase P complex and ELAC2, the importance of RNA processing (Brzezniak et al., 2011; Holzmann et al., 2008; Sanchez et al., 2011) and the consequences of its loss have not been investigated in vivo. Here, we investigated the loss of tRNA 5′ end processing upon conditional heart- and muscle-specific knockout of the *Mrpp3* gene, encoding the endonuclease component of the mitochondrial RNase P complex. We show that RNA processing is essential for early embryo development, and its knockout in the heart and skeletal muscle leads to very early onset cardiomyopathy that causes the mice to die by 11 weeks. Clearly, RNA processing is essential for life since severely impaired biogenesis of mitochondrial ribosomes and OXPHOS complexes leads to mitochondrial dysfunction. Our data further corroborate in vitro findings (Holzmann et al., 2008) and demonstrate that there are no alternative RNase P enzymes to compensate for the loss of the 5′ endonuclease activity of MRPP3. Impaired RNA processing has been shown recently due to mutation of the *MRPP1*, *MRPP2*, and *ELAC2* genes in patients with mitochondrial disease and cardiomyopathy (Haack et al., 2013; Metodiev et al., 2016; Vilardo and Rossmanith, 2015). Interestingly, in all three cases although RNA processing was shown to be impaired there was not a significant effect on the mature mtRNA levels, which is particularly curious. These effects may be a consequence of growth of patient cells in vitro in highly anaerobic conditions or the tissue-specific response of fibroblasts compared to heart and muscle cells and tissues, both of which do not impose the same bioenergetic requirements as in vivo systems. The requirement for RNA processing for life results in the observation of very mild hypomorphic mutations in these genes, masking the deleterious effects on RNA metabolism and making these effects difficult to detect in these patients.

Loss of MRPP3 in vivo abolishes tRNA 5′ end processing, trapping the individual mtRNAs in precursor transcripts and thereby

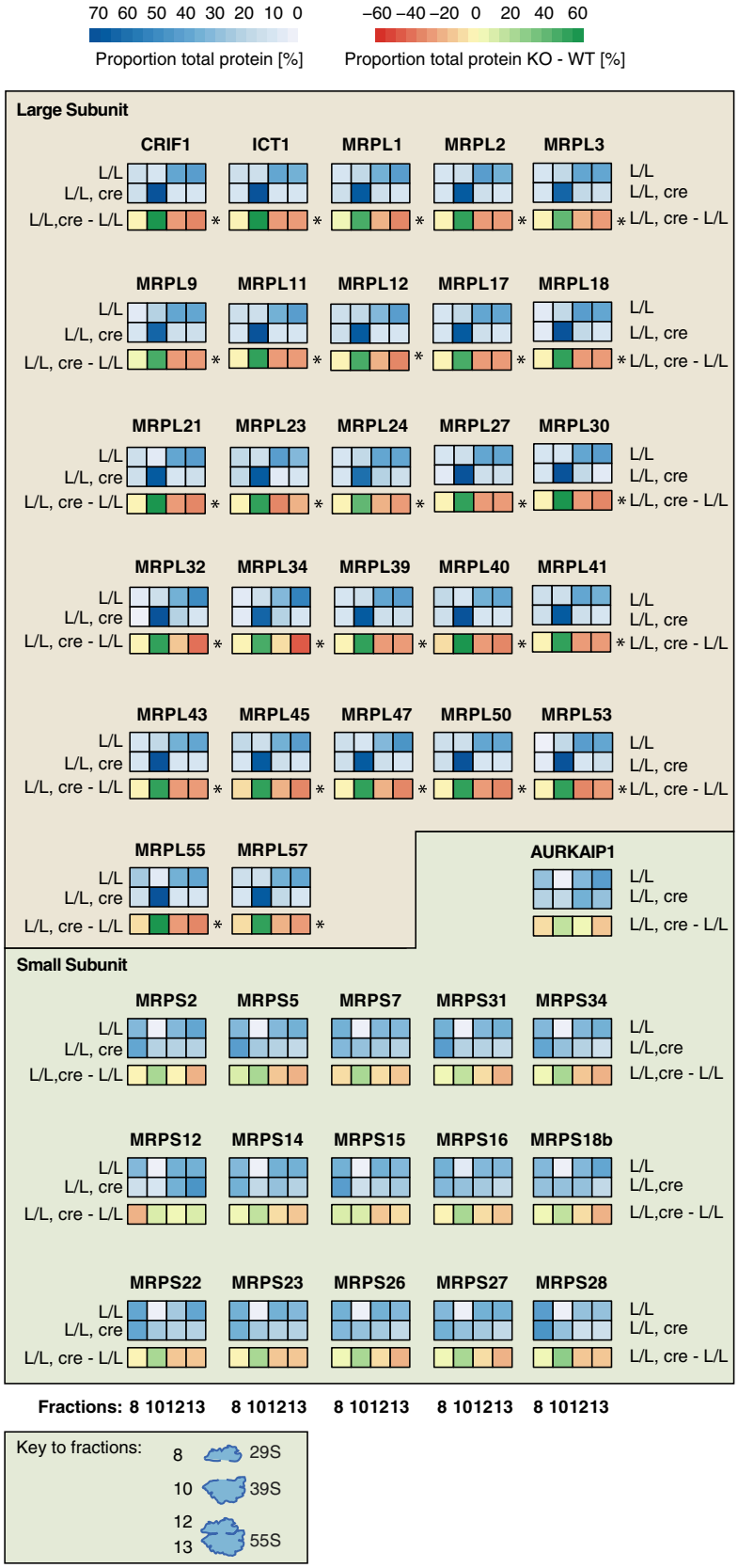

Figure 7. Differential Distribution of Mitochondrial Ribosomal Proteins upon Loss of MRPP3

Mass spectrometry was used to analyze the distribution of the mitochondrial ribosomal proteins in sucrose gradient fractions that contained the small (fraction 8) and large ribosomal subunit (fraction 10) and the monosome (fractions 12 and 13) in the control (L/L) mice and compared to the same fractions in the *Mrpp3* knockout mice (L/L, cre), both at 11 weeks. The analyses were performed on fractions from three separate biological experiments from three control and three knockout mice (n = 3). The results of the ANOVA analysis were adjusted for multiple testing using the Benjamini and Hochberg procedure. Only proteins with adjusted p value of less than 0.01 (1% FDR) were termed significant and marked with asterisk (*).

leads to profound reduction of most mature mtRNAs. The position of specific tRNAs or mRNAs within or adjacent to clusters of tRNA genes suggested that perhaps the activity of ELAC2 could rescue some of these transcripts by cleaving neighboring 3′ ends as we observed for *mt-Nd5*. However, this was not the case for the rRNAs where we found large unprocessed transcripts that precluded the correct assembly of the small and large ribosomal subunits. Although the levels of ELAC2 were moderately increased when MRPP3 was lost, they were not sufficient to rescue the processing of specific 3′ end sites that are also 5′ ends of flanking RNAs. We conclude that tRNA 5′ end processing is required as the initial step of RNA processing preceding 3′ tRNA cleavage. It is not clear why 5′ processing is required in most cases for 3′ processing to proceed, perhaps because the MRPP3 enzyme is more agnostic to structure, while RNase Z activity is inhibited by long 5′ leaders both for tRNA processing (Nashimoto et al., 1999) and cleavage of tRNA-like RNAs (Wilusz et al., 2008).

Interestingly, we identify two different sites that are not changed by the loss of MRPP3, one at the 5′ end of *mt-Cyt b* and the other at the 5′ end of *mt-Co3*. A gene trap mutant of the *Ptcd2* gene in mice has shown that the 5′ end of *mt-Cyt b* is not processed in the absence of PTCD2, suggesting that this protein may have a role in its cleavage (Xu et al., 2008). PTCD2 belongs to the PPR family of mitochondrial RNA-binding proteins in animals; like MRPP3, however besides its PPRs it lacks a canonical endoribonuclease domain, suggesting that there may be a new fold within its tertiary structure that can carry out this activity or that it recruits an unidentified endoribonuclease that can cleave this site. PPR proteins across different kingdoms can interact and recruit other RNA-binding proteins for their activity, such as the RNase P complex with the MRPP1 and MRPP2 (Holzmann et al., 2008; Li et al., 2015; Reinhard et al., 2015) and the LRPPRC/SLIRP complex (Lagouge et al., 2015; Ruzzenente et al., 2012; Sasarman et al., 2010) in animals or PPR proteins and MORF proteins in plants (Takenaka et al., 2012).

We annotated all the known MRPP3 cleavage sites in our work, accounting for all in vivo processing events carried out by the RNase P complex. Furthermore, we observed a dramatic increase in 5′ ends within internal regions of mtRNAs upon loss of MRPP3 and 5′ end processing. These are likely products of RNA degradation, and the general loss of these transcripts at their 3′ ends suggests that degradation is in the 3′ to 5′ direction. It remains to be determined which mitochondrial endonuclease is responsible for this removal of unprocessed RNAs, and a recent report suggests that LACTB2 may act as a mitochondrial endonuclease (Levy et al., 2016).

Mitochondrial gene expression relies solely on the post-transcriptional import of nuclear-encoded RNA-binding proteins and other protein factors (Hällberg and Larsson, 2014; Rackham et al., 2012). Knockout of mitochondrial RNA-binding proteins has been shown to increase the levels of other nuclear-encoded factors in an effort to compensate for the changes in gene expression (Cámara et al., 2011; Metodiev et al., 2009, 2014; Park et al., 2007; Ruzzenente et al., 2012). We observed similar increases in RNA-binding protein levels upon MRPP3 loss, but most strikingly we observed a dramatic increase in POLRMT levels and mitochondrial transcription. Furthermore, the varying effects on the mitochondrial ribosomal proteins suggested that the expression and stability of these proteins is differentially regulated. Nevertheless the dramatic changes that result from impaired tRNA 5′ end cleavage on transcription and protein synthesis indicate that RNA processing couples these two processes.

The cleavage of the 5′ ends of tRNAs is essential for ribosome assembly, which, in turn, is clearly a process that links transcription and translation. In addition, it indicates that it is the initial step of RNA processing, since ELAC2 and any other endoribonucleases cannot overcome the lack of 5′ processing. The small subunit is dependent on the mature 12S rRNA for assembly because its assembly is severely impaired in the *Mrpp3* knockout mice, and consequently the 55S ribosome cannot form. This may indicate that correctly processed 5′ and 3′ ends are required to initiate the early assembly events in small subunit formation. This mirrors bacterial ribosome assembly where the 5′ and 3′ ends of the 16S and 23S rRNAs must juxtapose for efficient ribosome biogenesis (Young and Steitz, 1978). However, it is interesting to note that a large subunit subcomplex can form using an unprocessed 16S rRNA and contains a number of large ribosomal subunit proteins, suggesting that some ribosomal proteins can assemble without the requirement for 16S rRNA processing. This is highly unusual, although the mitochondrial ribosome is unique in that it contains a much higher protein content compared to rRNA, as well as additional ribosomal proteins that are not found in cytoplasmic or prokaryotic ribosomes (Rackham and Filipovska, 2014b; Suzuki et al., 2001a, 2001b), suggesting that some of these could have unusual characteristics that may allow them to initiate binding or their stabilization by association with the unprocessed RNA. The MRPP3 knockout mouse has been useful to identify the ribosomal proteins involved in the initial assembly of the large mitochondrial ribosomal subunit, as the rRNAs become available following transcription. Taken together, we have shown that RNA processing is rate limiting for the assembly of the mitochondrial ribosomal subunits that occurs co-transcriptionally.

Here, we have shown the dire consequences of impaired mitochondrial RNA processing and that this is an essential step in mitochondrial RNA metabolism required for biogenesis and energy production. The next goal is to elucidate the precise mode of ribosome assembly that is clearly dependent on the generation of mature rRNAs. This will undoubtedly be a long and interesting journey with additional complexities as this tiny but mighty transcriptome has revealed so far.

EXPERIMENTAL PROCEDURES

Animals and Housing

Mrpp3 transgenic mice on a C57BL/6N background were generated by Taconic. The puromycin cassette was removed by mating $Mrpp3^{+/loxP\text{-}neo}$ mice with transgenic mice ubiquitously expressing Flp recombinase. The resulting $Mrpp3^{+/loxP}$ mice were mated with mice ubiquitously expressing Cre recombinase to generate heterozygous knockout $Mrpp3^{+/-}$ mice that were bred with each other to identify that the homozygous loss of *Mrpp3* was embryonic lethal. Heart- and skeletal muscle-specific knockout mice were generated by crossing $Mrpp3^{loxP/loxP}$ mice with transgenic mice expressing Cre under the control of the muscle creatinine kinase promoter (*Ckmm-cre*). Double

heterozygous mice (*Mrpp3*$^{loxP/+}$, +/*Ckmm-cre*) were mated with *Mrpp3*$^{loxP/loxP}$ mice to generate heart-specific knockout (*Mrpp3*$^{loxP/loxP}$, +/*Ckmm-cre*) and control mice (*Mrpp3*$^{loxP/loxP}$). Mice were housed in standard cages (45 cm × 29 cm × 12 cm) under a 12-hr light/dark schedule (lights on 7 a.m. to 7 p.m.) in controlled environmental conditions of 22 ± 2°C and 50 + 10% relative humidity and fed a normal chow diet (Rat & Mouse Chow, Specialty Foods) and water were provided ad libitum. The study was approved by the Animal Ethics Committee of the University of Western Australia (UWA) and performed in accordance with Principles of Laboratory Care (National Health and Medical Research Council [NHMRC] Australian code for the care and use of animals for scientific purposes, 8th Edition 2013) and Federation for Laboratory Animal Science Associations (FELASA), Germany.

Mitochondrial Isolation

Mitochondria were isolated from homogenized hearts and isolated by differential centrifugation as described previously (Lagouge et al., 2015; Mourier et al., 2014), with some modifications as described in the Supplemental Information.

Sucrose Gradient Fractionation

Sucrose gradient fractionation was carried out as described previously (Lagouge et al., 2015; Metodiev et al., 2009; Ruzzenente et al., 2012) with some modifications as described in the Supplemental Information.

Immunoblotting

Specific proteins were detected using rabbit polyclonal antibodies against POLRMT, LRPPRC, TFB2M, TFAM, ATP8 (produced in-house, diluted 1:1,000), MRPP1, MRPP2, ELAC2, MRPL44, MRPL37 (1:1,000), MRPL12 (1:500), MRPS35 (1:1,000), MRPS16 (Proteintech), and MRPS34 (Sigma, diluted 1:1,000) and mouse monoclonal antibodies against β-actin, voltage-dependent anion channel (VDAC), NDUFA9, complex II, complex III, COXI, COXII, COXIV, and complex V subunit a (Abcam, diluted 1:1,000), in Odyssey Blocking Buffer (Li-COR Biosciences). IR Dye 800CW goat anti-rabbit immunoglobulin G (IgG) or IRDye 680LT goat anti-mouse igg (Li-COR Biosciences) secondary antibodies were used, and the immunoblots were visualized using an Odyssey Infrared Imaging System (Li-COR Biosciences).

Mass Spectrometric Data Analyses

Protein and peptide identification was performed using Peaks (Ma et al., 2003) v.7.5. Raw data were searched against the canonical and isoform sequences of the mouse reference proteome (proteome ID UP000000589, June 2014) from UniProt. For data analysis, cysteine carbamidomethylation was set as "fixed modification" and methionine oxidation and protein N-terminal acetylation as "variable modification." The digestion parameters were set to "Trypsin" allowing for cleavage after lysine and arginine when not followed by proline with up to two missed cleavages. Database searching was performed using mass error tolerance of 10 ppm (parent) and 0.4 Da (fragment). Up to two variable modifications per peptide were allowed, and false discovery rate (FDR) estimation was enabled. Upon database searching, the peptide identification FDR was set at 1%; default criteria were used for protein identification. Peaks database search results were exported and used further for peptide and protein quantification. Label-free quantification was performed using Skyline (v.3.5.0.9319) (MacLean et al., 2010) using the MS1 filtering approach (Schilling et al., 2012). For the analyses, the peptides.pep.xml Peaks export file and a custom fasta database containing the sequences of all identified mitoribosomal proteins were imported into Skyline. For the fasta database import, "Trypsin [KR | P]" was set as a protease allowing for up to two missed cleavages. Regarding the full-scan settings, the precursor charges were set to two, three, and four. MS1 filtering was performed using three peaks (M, M+1 and M+2), "Orbitrap" was selected as a mass analyzer with resolving power of 60,000 at 200 m/z. Only scans within 5 min of MS/MS IDs were considered. After data import, the extracted ion chromatograms of all peptides mapping to the selected mitoribosomal proteins were manually inspected. In some cases, the peak integration was adjusted manually. When no distinct peak was present, data integration was performed over a retention time region, which is in agreement with the replicated analysis of the same and the remaining fractions. Upon manual evaluation, the peptide intensity data were exported and assembled into protein intensity data using an in-house script. Similarly to other label-free approaches (Wiśniewski and Rakus, 2014), protein intensities in all four fractions were transformed into proportions of the total protein intensity in all four fractions, in order to derive the relative distribution of a protein in the gradient fractions. The proportion values in each fraction were used to perform a two-way ANOVA analysis using two factors, "Genotype," "Fraction," and their interaction. The ANOVA analysis was performed in R (R Development Core Team, 2013, http://www.r-project.org/), using the analysis of variance (aov) function. The results of the ANOVA analysis were adjusted for multiple testing using the Benjamini and Hochberg procedure (Benjamini and Hochberg, 1995). Only proteins with adjusted p value of less than 0.01 (1% FDR) were termed significant.

RNA Isolation, Northern Blotting, and qRT-PCR

RNA was isolated from total hearts or heart mitochondria using the miRNeasy Mini kit (QIAGEN) incorporating an on-column RNase-free DNase digestion to remove all DNA. RNA (5 μg) was resolved on 1.2% agarose formaldehyde gels and then transferred to 0.45 μm Hybond-N^+ nitrocellulose membrane (GE Healthcare Life Sciences) and hybridized with biotinylated oligonucleotide probes specific to mouse mitochondrial mRNAs, rRNAs, and tRNAs (Rackham et al., 2009). Hybridizations were carried out overnight at 50°C in 5× saline sodium citrate (SSC), 20 mM Na_2HPO_4, 7% SDS, and 100 μg × ml^{-1} heparin, followed by washing. The signal was detected using either streptavidin-linked horseradish peroxidase or streptavidin-linked infrared-labeled antibody (diluted 1:2,000 in 3× SSC, 5% SDS, 25 mM Na_2HPO_4 [pH 7.5]) by enhanced chemiluminescence (GE Healthcare Life Sciences) or using an Odyssey Infrared Imaging System (Li-COR Biosciences), respectively.

cDNA was prepared using the QuantiTect Reverse Transcription Kit (QIAGEN) and used as a template in the subsequent PCR that was performed using a Corbett Rotorgene 6000 using SensiMix SYBR mix (Bioline) and normalized to 18S rRNA.

RNA-Seq, PARE, and Alignments

RNA sequencing was performed on total RNA or mitochondrial RNA from three control and three *Mrpp3* knockout mice using the Illumina HiSeq platform, according to the Illumina Tru-Seq protocol or PARE protocol (German et al., 2009; Mercer et al., 2011; Rackham and Filipovska, 2014a). Library preparation, sequencing, and bioinformatics analyses are described in detail in the Supplemental Information.

Transcription and Translation Assays

In organello transcription and translation assays were carried out in isolated heart mitochondria as described before (Lagouge et al., 2015).

Blue Native PAGE

BN-PAGE was carried out using isolated mitochondria from hearts as described previously (Mourier et al., 2014). BN-PAGE gels were analyzed by in-gel activity assays or by transferring to polyvinylidene fluoride (PVDF) and immunoblotting against the respiratory complexes.

Respiratory Chain Function and Complex Activity

The mitochondrial oxygen consumption flux was measured with an Oxygraph-2k (Oroboros Instruments), as previously described (Mourier et al., 2014; Lagouge et al., 2015).

Histology

Mouse hearts were fixed with 10% neutral buffered formalin for 24 hr and stored in PBS or 70% ethanol. Tissues were embedded in paraffin, sectioned using a microtome, and transferred to positively charged slides. Slides were heated for 2 hr at 60°C and treated with xylene, xylene and ethanol (1:1), and decreasing concentrations of ethanol (100%, 95%, 80%, 60%) before they were washed in distilled H_2O (dH_2O). The H&E staining was performed as described before (Richman et al., 2015). Skeletal muscle was frozen in OCT, and the tissue was sectioned and stained for complex I and IV activity using NADH and cytochrome *c* oxidase as substrates. Coverslips were attached using DPX mounting media (Scharlau) and images were acquired using a Nikon Ti Eclipse inverted microscope using a Nikon 20× objective.

ACCESSION NUMBERS

The accession number for the RNA-seq and PARE data reported in this paper is Gene Expression Omnibus (GEO): GSE83471.

SUPPLEMENTAL INFORMATION

Supplemental Information includes Supplemental Experimental Procedures, four figures, and two tables and can be found with this article online at http://dx.doi.org/10.1016/j.celrep.2016.07.031.

AUTHOR CONTRIBUTIONS

O.R., N.-G.L., and A.F. conceived the project and designed the experiments. O.R., J.D.B., S.M., S.S., I.K., I.A., J.A.E., A.-M.J.S., T.R.R., J.B.S., A.M., D.M., and A.F. conducted and analyzed the experiments. O.R. and A.F. wrote the manuscript, and the other authors approved the manuscript.

ACKNOWLEDGMENTS

This project was supported by fellowships and project grants from the National Health and Medical Research Council (APP1058442, APP1045677, APP1041582, APP1023460, APP1005030, APP1043978 to A.F. and O.R.), Australian Research Council (to A.F. and O.R.), the Cancer Council of Western Australia (to O.R.), Swedish Research Council (Rådsprofessor 2015–0418 to N.-G.L.), Knut and Alice Wallenbergs Foundation (to N.-G.L.), and the Alexander von Humboldt Foundation (to A.F., O.R., and N.-G.L.). S.M. was supported by an EMBO Short-Term Scholarship. We thank Lysann Schmitz, Julia Preilowski, and Maike Stentenbach for technical assistance, Dr. Min Jiang for advice on the embryo isolation and Dr. Jorge Boucas for help with the bioinformatics pipeline for analyses of the transcriptome-wide differential expression.

Received: May 18, 2016
Revised: June 20, 2016
Accepted: July 13, 2016
Published: August 4, 2016

REFERENCES

Antonicka, H., and Shoubridge, E.A. (2015). Mitochondrial RNA Granules Are Centers for Posttranscriptional RNA Processing and Ribosome Biogenesis. Cell Reports *10*, 920–932.

Benjamini, Y., and Hochberg, Y. (1995). Controlling the false discovery rate - a practical and powerful approach to multiple testing. J. R. Stat. Soc. Series B Stat. Methodol. *57*, 289–300.

Brzezniak, L.K., Bijata, M., Szczesny, R.J., and Stepien, P.P. (2011). Involvement of human ELAC2 gene product in 3′ end processing of mitochondrial tRNAs. RNA Biol. *8*, 616–626.

Cámara, Y., Asin-Cayuela, J., Park, C.B.C., Metodiev, M.D.M., Shi, Y., Ruzzenente, B., Kukat, C., Habermann, B., Wibom, R., Hultenby, K., et al. (2011). MTERF4 regulates translation by targeting the methyltransferase NSUN4 to the mammalian mitochondrial ribosome. Cell Metab. *13*, 527–539.

Davies, S.M.K., Rackham, O., Shearwood, A.-M.J., Hamilton, K.L., Narsai, R., Whelan, J., and Filipovska, A. (2009). Pentatricopeptide repeat domain protein 3 associates with the mitochondrial small ribosomal subunit and regulates translation. FEBS Lett. *583*, 1853–1858.

Davies, S.M.K., Lopez Sanchez, M.I.G., Narsai, R., Shearwood, A.-M.J., Razif, M.F.M., Small, I.D., Whelan, J., Rackham, O., and Filipovska, A. (2012). MRPS27 is a pentatricopeptide repeat domain protein required for the translation of mitochondrially encoded proteins. FEBS Lett. *586*, 3555–3561.

Dogan, S.A., Pujol, C., Maiti, P., Kukat, A., Wang, S., Hermans, S., Senft, K., Wibom, R., Rugarli, E.I., and Trifunovic, A. (2014). Tissue-specific loss of DARS2 activates stress responses independently of respiratory chain deficiency in the heart. Cell Metab. *19*, 458–469.

Duff, R.M., Shearwood, A.-M.J., Ermer, J., Rossetti, G., Gooding, R., Richman, T.R., Balasubramaniam, S., Thorburn, D.R., Rackham, O., Lamont, P.J., and Filipovska, A. (2015). A mutation in MT-TW causes a tRNA processing defect and reduced mitochondrial function in a family with Leigh syndrome. Mitochondrion *25*, 113–119.

German, M.A., Luo, S., Schroth, G., Meyers, B.C., and Green, P.J. (2009). Construction of parallel analysis of RNA ends (PARE) libraries for the study of cleaved miRNA targets and the RNA degradome. Nat. Protoc. *4*, 356–362.

Gobert, A., Gutmann, B., Taschner, A., Gössringer, M., Holzmann, J., Hartmann, R.K., Rossmanith, W., and Giegé, P. (2010). A single Arabidopsis organellar protein has RNase P activity. Nat. Struct. Mol. Biol. *17*, 740–744.

Haack, T.B., Kopajtich, R., Freisinger, P., Wieland, T., Rorbach, J., Nicholls, T.J., Baruffini, E., Walther, A., Danhauser, K., Zimmermann, F.A., et al. (2013). ELAC2 mutations cause a mitochondrial RNA processing defect associated with hypertrophic cardiomyopathy. Am. J. Hum. Genet. *93*, 211–223.

Hällberg, B.M., and Larsson, N.-G. (2014). Making proteins in the powerhouse. Cell Metab. *20*, 226–240.

Holzmann, J., Frank, P., Löffler, E., Bennett, K.L., Gerner, C., and Rossmanith, W. (2008). RNase P without RNA: identification and functional reconstitution of the human mitochondrial tRNA processing enzyme. Cell *135*, 462–474.

Kühl, I., Kukat, C., Ruzzenente, B., Milenkovic, D., Mourier, A., Miranda, M., Koolmeister, C., Falkenberg, M., and Larsson, N.-G. (2014). POLRMT does not transcribe nuclear genes. Nature *514*, E7–E11.

Lagouge, M., Mourier, A., Lee, H.J., Spåhr, H., Wai, T., Kukat, C., Silva Ramos, E., Motori, E., Busch, J.D., Siira, S., et al.; German Mouse Clinic Consortium (2015). SLIRP regulates the rate of mitochondrial protein synthesis and protects LRPPRC from degradation. PLoS Genet. *11*, e1005423.

Larsson, N.-G., Wang, J., Wilhelmsson, H., Oldfors, A., Rustin, P., Lewandoski, M., Barsh, G.S., and Clayton, D.A. (1998). Mitochondrial transcription factor A is necessary for mtDNA maintenance and embryogenesis in mice. Nat. Genet. *18*, 231–236.

Levy, S., Allerston, C.K., Liveanu, V., Habib, M.R., Gileadi, O., and Schuster, G. (2016). Identification of LACTB2, a metallo-β-lactamase protein, as a human mitochondrial endoribonuclease. Nucleic Acids Res. *44*, 1813–1832.

Li, F., Liu, X., Zhou, W., Yang, X., and Shen, Y. (2015). Auto-inhibitory mechanism of the human mitochondrial RNase P protein complex. Sci. Rep. *5*, 9878.

Liu, G., Mercer, T.R., Shearwood, A.-M.J., Siira, S.J., Hibbs, M.E., Mattick, J.S., Rackham, O., and Filipovska, A. (2013). Mapping of mitochondrial RNA-protein interactions by digital RNase footprinting. Cell Rep. *5*, 839–848.

Ma, B., Zhang, K., Hendrie, C., Liang, C., Li, M., Doherty-Kirby, A., and Lajoie, G. (2003). PEAKS: powerful software for peptide de novo sequencing by tandem mass spectrometry. Rapid Commun. Mass Spectrom. *17*, 2337–2342.

MacLean, B., Tomazela, D.M., Shulman, N., Chambers, M., Finney, G.L., Frewen, B., Kern, R., Tabb, D.L., Liebler, D.C., and MacCoss, M.J. (2010). Skyline: an open source document editor for creating and analyzing targeted proteomics experiments. Bioinformatics *26*, 966–968.

Mercer, T.R., Neph, S., Dinger, M.E., Crawford, J., Smith, M.A., Shearwood, A.-M.J., Haugen, E., Bracken, C.P., Rackham, O., Stamatoyannopoulos, J.A., et al. (2011). The human mitochondrial transcriptome. Cell *146*, 645–658.

Metodiev, M.D., Lesko, N., Park, C.B., Cámara, Y., Shi, Y., Wibom, R., Hultenby, K., Gustafsson, C.M., and Larsson, N.-G. (2009). Methylation of 12S rRNA is necessary for in vivo stability of the small subunit of the mammalian mitochondrial ribosome. Cell Metab. *9*, 386–397.

Metodiev, M.D., Spåhr, H., Loguercio Polosa, P., Meharg, C., Becker, C., Altmueller, J., Habermann, B., Larsson, N.-G., and Ruzzenente, B. (2014). NSUN4 is a dual function mitochondrial protein required for both methylation of 12S rRNA and coordination of mitoribosomal assembly. PLoS Genet. *10*, e1004110.

Metodiev, M.D., Thompson, K., Alston, C.L., Morris, A.A., He, L., Assouline, Z., Rio, M., Bahi-Buisson, N., Pyle, A., Griffin, H., et al. (2016). Recessive mutations in *TRMT10C* cause defects in mitochondrial RNA processing and multiple respiratory chain deficiencies. Am. J. Hum. Genet. *98*, 993–1000.

Montoya, J., Ojala, D., and Attardi, G. (1981). Distinctive features of the 5′-terminal sequences of the human mitochondrial mRNAs. Nature *290*, 465–470.

Mourier, A., Ruzzenente, B., Brandt, T., Kühlbrandt, W., and Larsson, N.-G. (2014). Loss of LRPPRC causes ATP synthase deficiency. Hum. Mol. Genet. *23*, 2580–2592.

Nashimoto, M., Wesemann, D.R., Geary, S., Tamura, M., and Kaspar, R.L. (1999). Long 5′ leaders inhibit removal of a 3′ trailer from a precursor tRNA by mammalian tRNA 3′ processing endoribonuclease. Nucleic Acids Res. *27*, 2770–2776.

Ojala, D., Montoya, J., and Attardi, G. (1981). tRNA punctuation model of RNA processing in human mitochondria. Nature *290*, 470–474.

Okui, S., Ushida, C., Kiyosawa, H., and Kawai, G. (2016). Sequence and structure analysis of a mirror tRNA located upstream of the cytochrome oxidase I mRNA in mouse mitochondria. J. Biochem. *159*, 341–350.

Park, C.B., Asin-Cayuela, J., Cámara, Y., Shi, Y., Pellegrini, M., Gaspari, M., Wibom, R., Hultenby, K., Erdjument-Bromage, H., Tempst, P., et al. (2007). MTERF3 is a negative regulator of mammalian mtDNA transcription. Cell *130*, 273–285.

R Development Core Team (2013). The R project for statistical computing (R Foundation for Statistical Computing).

Rackham, O., and Filipovska, A. (2014a). Analysis of the human mitochondrial transcriptome using directional deep sequencing and parallel analysis of RNA ends. Methods Mol Biol. *1125*, 263–275.

Rackham, O., and Filipovska, A. (2014b). Supernumerary proteins of mitochondrial ribosomes. Biochim. Biophys. Acta *1840*, 1227–1232.

Rackham, O., Davies, S.M.K., Shearwood, A.-M.J., Hamilton, K.L., Whelan, J., and Filipovska, A. (2009). Pentatricopeptide repeat domain protein 1 lowers the levels of mitochondrial leucine tRNAs in cells. Nucleic Acids Res. *37*, 5859–5867.

Rackham, O., Mercer, T.R., and Filipovska, A. (2012). The human mitochondrial transcriptome and the RNA-binding proteins that regulate its expression. Wiley Interdiscip. Rev. RNA *3*, 675–695.

Reinhard, L., Sridhara, S., and Hällberg, B.M. (2015). Structure of the nuclease subunit of human mitochondrial RNase P. Nucleic Acids Res. *43*, 5664–5672.

Richman, T.R., Ermer, J.A., Davies, S.M.K., Perks, K.L., Viola, H.M., Shearwood, A.-M.J., Hool, L.C., Rackham, O., and Filipovska, A. (2015). Mutation in MRPS34 compromises protein synthesis and causes mitochondrial dysfunction. PLoS Genet. *11*, e1005089.

Ruzzenente, B., Metodiev, M.D., Wredenberg, A., Bratic, A., Park, C.B., Cámara, Y., Milenkovic, D., Zickermann, V., Wibom, R., Hultenby, K., et al. (2012). LRPPRC is necessary for polyadenylation and coordination of translation of mitochondrial mRNAs. EMBO J. *31*, 443–456.

Sanchez, M.I., Mercer, T.R., Davies, S.M., Shearwood, A.-M.J., Nygård, K.K., Richman, T.R., Mattick, J.S., Rackham, O., and Filipovska, A. (2011). RNA processing in human mitochondria. Cell Cycle *10*, 2904–2916.

Sasarman, F., Brunel-Guitton, C., Antonicka, H., Wai, T., and Shoubridge, E.A.; LSFC Consortium (2010). LRPPRC and SLIRP interact in a ribonucleoprotein complex that regulates posttranscriptional gene expression in mitochondria. Mol. Biol. Cell *21*, 1315–1323.

Schilling, B., Rardin, M.J., MacLean, B.X., Zawadzka, A.M., Frewen, B.E., Cusack, M.P., Sorensen, D.J., Bereman, M.S., Jing, E., Wu, C.C., et al. (2012). Platform-independent and label-free quantitation of proteomic data using MS1 extracted ion chromatograms in skyline: application to protein acetylation and phosphorylation. Mol. Cell. Proteomics *11*, 202–214.

Small, I.D., Rackham, O., and Filipovska, A. (2013). Organelle transcriptomes: products of a deconstructed genome. Curr. Opin. Microbiol. *16*, 652–658.

Suzuki, T., Terasaki, M., Takemoto-Hori, C., Hanada, T., Ueda, T., Wada, A., and Watanabe, K. (2001a). Proteomic analysis of the mammalian mitochondrial ribosome. Identification of protein components in the 28 S small subunit. J. Biol. Chem. *276*, 33181–33195.

Suzuki, T., Terasaki, M., Takemoto-Hori, C., Hanada, T., Ueda, T., Wada, A., and Watanabe, K. (2001b). Structural compensation for the deficit of rRNA with proteins in the mammalian mitochondrial ribosome. Systematic analysis of protein components of the large ribosomal subunit from mammalian mitochondria. J. Biol. Chem. *276*, 21724–21736.

Takenaka, M., Zehrmann, A., Verbitskiy, D., Kugelmann, M., Härtel, B., and Brennicke, A. (2012). Multiple organellar RNA editing factor (MORF) family proteins are required for RNA editing in mitochondria and plastids of plants. Proc. Natl. Acad. Sci. USA *109*, 5104–5109.

Taschner, A., Weber, C., Buzet, A., Hartmann, R.K., Hartig, A., and Rossmanith, W. (2012). Nuclear RNase P of Trypanosoma brucei: a single protein in place of the multicomponent RNA-protein complex. Cell Rep. *2*, 19–25.

Vilardo, E., and Rossmanith, W. (2015). Molecular insights into HSD10 disease: impact of SDR5C1 mutations on the human mitochondrial RNase P complex. Nucleic Acids Res. *43*, 5112–5119.

Vilardo, E., Nachbagauer, C., Buzet, A., Taschner, A., Holzmann, J., and Rossmanith, W. (2012). A subcomplex of human mitochondrial RNase P is a bifunctional methyltransferase–extensive moonlighting in mitochondrial tRNA biogenesis. Nucleic Acids Res. *40*, 11583–11593.

Wilusz, J.E., Freier, S.M., and Spector, D.L. (2008). 3′ end processing of a long nuclear-retained noncoding RNA yields a tRNA-like cytoplasmic RNA. Cell *135*, 919–932.

Wiśniewski, J.R., and Rakus, D. (2014). Multi-enzyme digestion FASP and the 'Total Protein Approach'-based absolute quantification of the Escherichia coli proteome. J. Proteomics *109*, 322–331.

Xu, F., Ackerley, C., Maj, M.C., Addis, J.B., Levandovskiy, V., Lee, J., Mackay, N., Cameron, J.M., and Robinson, B.H. (2008). Disruption of a mitochondrial RNA-binding protein gene results in decreased cytochrome b expression and a marked reduction in ubiquinol-cytochrome c reductase activity in mouse heart mitochondria. Biochem. J. *416*, 15–26.

Young, R.A., and Steitz, J.A. (1978). Complementary sequences 1700 nucleotides apart form a ribonuclease III cleavage site in Escherichia coli ribosomal precursor RNA. Proc. Natl. Acad. Sci. USA *75*, 3593–3597.

Zschocke, J. (2012). HSD10 disease: clinical consequences of mutations in the HSD17B10 gene. J. Inherit. Metab. Dis. *35*, 81–89.